Medical Engineering and Physics 43 (2017) 1–18

Contents lists available at ScienceDirect

Medical Engineering and Physics

journal homepage: www.elsevier.com/locate/medengphy

# Finite element analysis of the amputated lower limb: A systematic review and recommendations

A.S. Dickinson[a,*], J.W. Steer[a], P.R. Worsley[b]

[a] Bioengineering Science Research Group, Faculty of Engineering and the Environment, University of Southampton, UK
[b] Clinical Academic Facility, Faculty of Health Sciences, University of Southampton, UK

ARTICLE INFO

*Article history:*
Received 20 October 2016
Revised 17 January 2017
Accepted 10 February 2017

*Keywords:*
FEA
Amputation
Prosthetics
Residual limb
Soft tissue stress
Deep tissue injury (DTI)
Pressure ulcers

ABSTRACT

The care and rehabilitation of individuals after lower limb amputation presents a substantial and growing socioeconomic challenge. Clinical outcome is closely linked to successful functional rehabilitation with a prosthetic limb, which depends upon comfortable prosthetic limb – residual limb load transfer. Despite early interest in the 1980s, the amputated limb has received considerably less attention in computational biomechanical analysis than other subjects, such as arthroplasty. This systematic literature review investigates the state of the art in residual limb finite element analysis published since 2000. The identified studies were grouped into the following categories: (1) residuum-prosthesis interface mechanics; (2) residuum soft tissue internal mechanics; (3) identification of residuum tissue characteristics; (4) proposals for incorporating FEA into the prosthesis fitting process; (5) analysis of the influence of prosthetic componentry concepts to improve load transfer to the residuum, such as the monolimb and structural socket compliance; and (6) analysis of osseointegrated (OI) prostheses. The state of the art is critically appraised in order to form recommendations for future modeling studies in terms of geometry, material properties, boundary conditions, interface models, and relevant but un-investigated issues. Finally, the practical implementation of these approaches is discussed.



## 1. Introduction

The care and rehabilitation of individuals after lower limb amputation presents a substantial and growing socioeconomic challenge. The International Society for Prosthetics and Orthotics reports that there is a recognized need for advanced technology in prosthetic limb componentry and its provision, and there is a desire in the clinical community to enhance evidence-based practice [1].

Rehabilitation after amputation commonly aims to restore functional independence through promotion of ambulation using a prosthetic limb. Fitting a conventional prosthetic limb employing a socket for suspension commonly requires an iterative and labor-intensive process [2,3]. This is partially a consequence of changes in the residual limb soft tissues, including their volume, shape, tissue composition, sensitivity, and scarring from surgical wounds. These factors may vary during the course of a day due to temperature, activity and hydration, or over several months, as postoperative oedema subsides, muscles atrophy and soft tissues remodel to enable socket-skeleton load transfer [4–6].

The extent and duration of comfortable load transfer to the residual limb changes during rehabilitation, and there are considerable challenges in identifying physiologically-informed biomechanical targets for the socket's design. Instead, prosthetists aim to produce an acceptable definitive socket by using their experience and patient feedback with iteratively adjusted trial sockets. Short term changes in the residuum are typically managed using socks and soft 'Pelite' polymer foam or silicone gel liners. However, ill-fitting sockets are still common for this population, affecting an individual's quality of life through discomfort and functional limitations, causing secondary musculoskeletal conditions such as osteoarthritis, osteoporosis, and lower back pain [7].

In below knee amputation (BKA) surgery, a soft tissue pad is created over the resected tibia and fibula comprising the gastrocnemius and soleus muscles. The pad is sutured to the anterior tibial periosteum or the bone, and a posterior or skewed flap of skin seals the site. When a conventional, socket-suspended prosthesis is used, the muscles, predominantly subject to tensile loading along the fiber direction, are therefore subject to shear and transverse compression. Strain concentrations are also experienced

* Corresponding author.
*E-mail addresses:* alex.dickinson@soton.ac.uk (A.S. Dickinson), joshua.steer@soton.ac.uk (J.W. Steer), p.r.worsley@soton.ac.uk (P.R. Worsley).

http://dx.doi.org/10.1016/j.medengphy.2017.02.008
1350-4533/

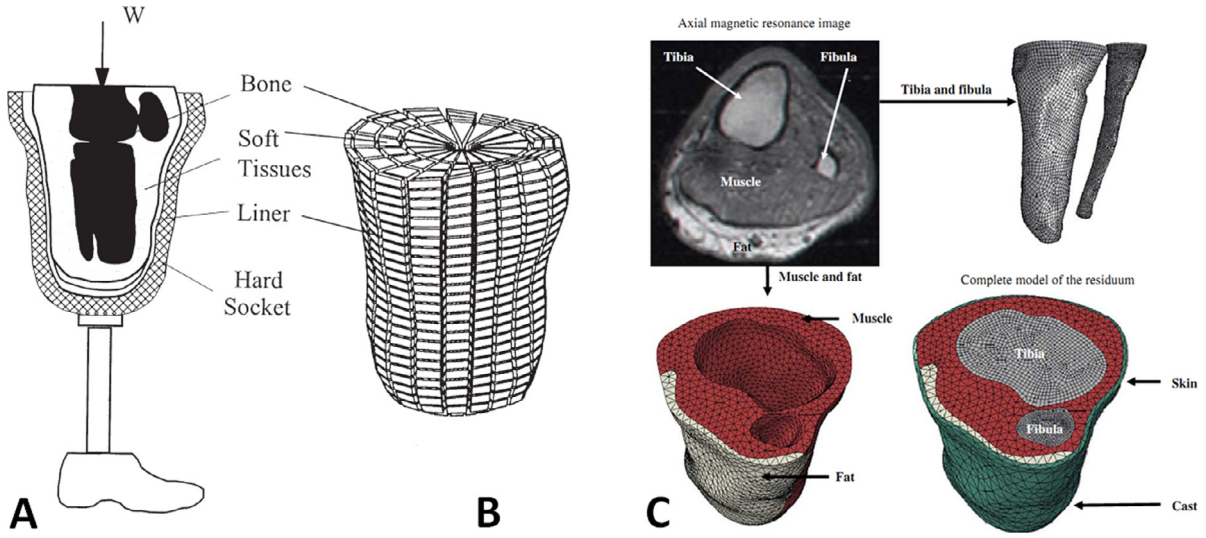


**Fig. 1.** Examples of published residual limb FE models, intended to represent loading through a prosthetic socket and liner with multiple bone models (A,B), and to represent an upright-MRI scan scenario loading through a plaster cast (C). Reproduced from: A,B) Reprinted from [26] with permission from Elsevier (license 3,973,140,409,695), and C) Reprinted from [46] with permission from Elsevier (license 3,973,140,811,893).

around bony prominences, such as the anterior edge of the tibia. Furthermore, the soft, relatively non-load bearing skin covering the calf, patella tendon, tibial plateau and anterior tibial surface becomes the primary load transmitting interface, and experiences substantial cyclic pressure and shear. In above knee amputation (AKA), similar changes in loading may be experienced by the skin and adductor muscles at the distal femur, and by the proximal soft tissues around the ischiopubic ramus and greater trochanter bony prominences. Alternatively, a prosthetic limb may be suspended by an implant, fixed directly to the residual bone by osseointegration (OI).

The residuum–prosthesis interface is the site at which the majority of early complications are observed during rehabilitation, and is directly influenced by the custom-designed prosthetic socket, liners and socks, and how they are used. The incidence of skin disorders is substantial [8], resulting from the requirement to transmit elevated compressive and shear forces between the prosthesis and residual limb. The residuum tissues are not used to bearing normal compressive and shear load, as the plantar tissues in the foot are [9,10]. Incorrect socket fit can potentially lead to dermatologic problems such as contact dermatitis [8] and keratosis [11], and in serious cases, internal tissue strain and ischemia can lead to deep tissue injury [12]. Discomfort and the risk of skin breakdown are elevated with a moist climate due to perspiration, and prolonged exposure to the chemical compounds of the prosthesis [13]. These problems can arise in established residual limbs with no history of skin problems as a result of changes in liner and socket prescription, as well as the environment at the interface. For example, the process by which patients apply a liner to their residual limbs prior to donning a socket may introduce trapped air, which can influence skin friction, temperature and potentially lead to blistering [14].

The residuum tissues must adapt to their changed mechanobiological duties, which is a lengthy and uncomfortable process. Important progress has been made towards understanding the tissues' sustainable threshold levels of strain magnitude and duration [15] the adaptive processes are highly variable, and not fully understood. Finite element analysis (FEA) is a type of numerical modeling which, when applied to the residual limb (Fig. 1) has potential to offer insights into soft tissue load distributions and magnitudes, which may provide an evidence base to assist prosthetists with socket design, allowing rehabilitation to be expedited with reduced discomfort and treatment expense [16]. It also enables pre-clinical analysis of novel prosthetic componentry, such as OI implant-suspended concepts.

This paper reports a systematic review of the literature, up to January 2017, considering the application of FEA methods to analyze the residual tissues in the amputated lower limb, and their interface with prosthetic componentry, nominally sockets, liners and osseointegrated implants. The review's objective was to identify the state of the art in numerical analysis considering recent trends in modeling approaches and objectives, experimental validation, interface models, tissue material models, derivation of anatomic geometry, and applied loading and boundary conditions. Furthermore, the range of study questions and model output measures was evaluated, and a discussion of future research possibilities is proposed. In order to facilitate this work, reference is made to a range of clinical reports which may provide appropriate model input data or be employed for modeling corroboration, and measurement techniques for validation. Finally, comments are made regarding the potential for practical implementation of these techniques to answer the prosthetic and orthotic community's needs.

## 2. Methodology

### 2.1. Search strategy

This systematic literature review employed the PRISMA (Preferred Reporting Items for Systematic reviews and Meta-Analyses) approach [17]. Two databases (Web of Science and PubMed) were searched for relevant articles using the following keywords:

**(finite element) AND ((transtibial OR trans-tibial OR below knee) OR (transfemoral OR trans-femoral OR above knee) OR disarticulation) AND (amput*)**

For each article, the reference lists and forward-citation reports from each database were consulted in order to identify additional relevant articles that were not found in the automatic search.

### 2.2. Study selection

Primary eligible articles were selected from the full list of automatically retrieved articles. This review aimed to capture original research involving finite element analysis of the residual lower limb following amputation. Therefore, review articles, and

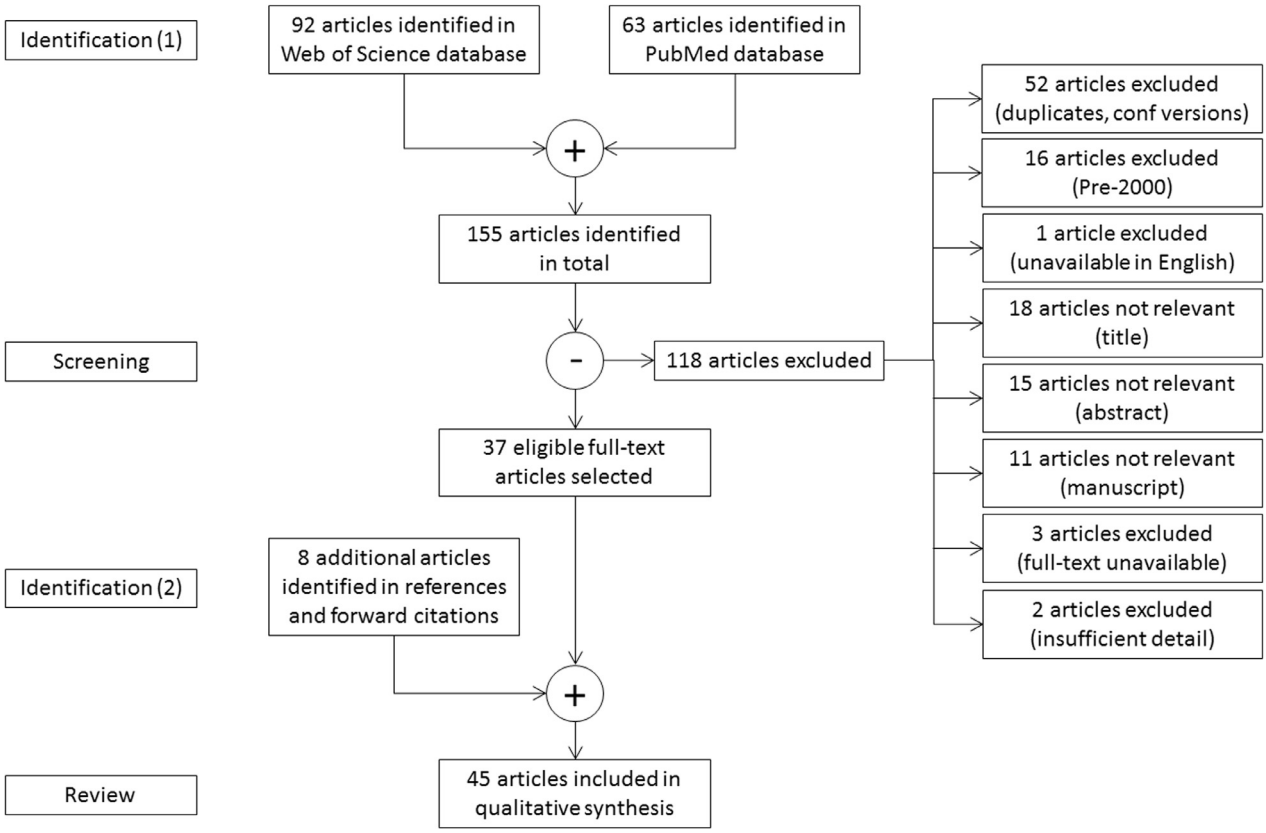


**Fig. 2.** Literature search process and results.

duplicate articles published as conference proceedings were excluded. Studies which performed FEA on the prosthesis without modeling the residual limb were excluded, but the search was not restricted to any particular prosthetic componentry type. Finally, studies were assessed for their methodological and results detail. Articles were excluded which did not offer quantitative details of material properties, loading and/or results. Triangulation between the three authors was used to verify the decisions to exclude articles.

Where the full text of an article was not available, the corresponding author was contacted by their current email address. A small number of non-English-language articles were identified, and again the corresponding author was contacted and a translated version, or an interpretation of the key study information was requested. In both situations, if no response was received within one month, the study was excluded.

Finally, in light of past reviews conducted on this subject, the search was restricted to studies published from the year 2000 onwards. Silver-Thorn et al. [18], and Zachariah and Sanders [19] produced reviews in 1996 including detailed analyses of prior FE modeling approaches, which were followed two years later by Zhang, et al. [20]. More recent review articles [21–25] have considered finite element analysis of the residuum and prosthesis as part of a wider remit, but provided valuable insight into the state of the art and scope for further research, which are presented in the Discussion section.

## 3. Results

### 3.1. Search results

On 14th September 2016, the automated search identified 92 articles in the Web of Science database, and 63 in the PubMed database. After screening to the eligibility criteria listed above, 39 eligible articles remained. Two more articles were excluded because they did not include sufficient details for full assessment. Through review of the eligible articles' reference lists and forward citation lists, a further 8 eligible articles were identified, giving a total of 45 articles (Fig. 2). The search was repeated one month later, and again on 1st January 2017 during the response to reviewers' comments, and no additional articles were identified.

### 3.2. Grouping

The articles were grouped by intervention (Fig. 3). The search yielded 25 articles on transtibial amputation since year 2000: [26–50]), 4 articles on conventional transfemoral amputation since 2000: [51–54]), and 16 on transfemoral amputation treated with an osseointegrated prosthesis since 2000: [55–70]). The search was robust against variants including 'exarticulation' and 'through-knee' in place of 'disarticulation'. The main observed trends in publication were a greater focus upon transtibial than transfemoral amputation, and a recent increase in osseointegrated prosthesis modeling, applied to AKA.

The post-2000 eligible articles were grouped by research focus into the following categories: (1) residuum–prosthesis interface mechanics (Table 1); (2) residuum soft tissue internal mechanics (Table 2); (3) identification of residuum tissue characteristics; (4) proposals for incorporating FEA into the prosthesis fitting process; (5) analysis of prosthetic componentry innovations; and (6) analysis of osseointegrated prostheses (Table 4). This grouping forms the structure of the Discussion. For each study, the pre- and post-processing parameters were identified (Fig. 4) so that trends in methodology and results could be identified.

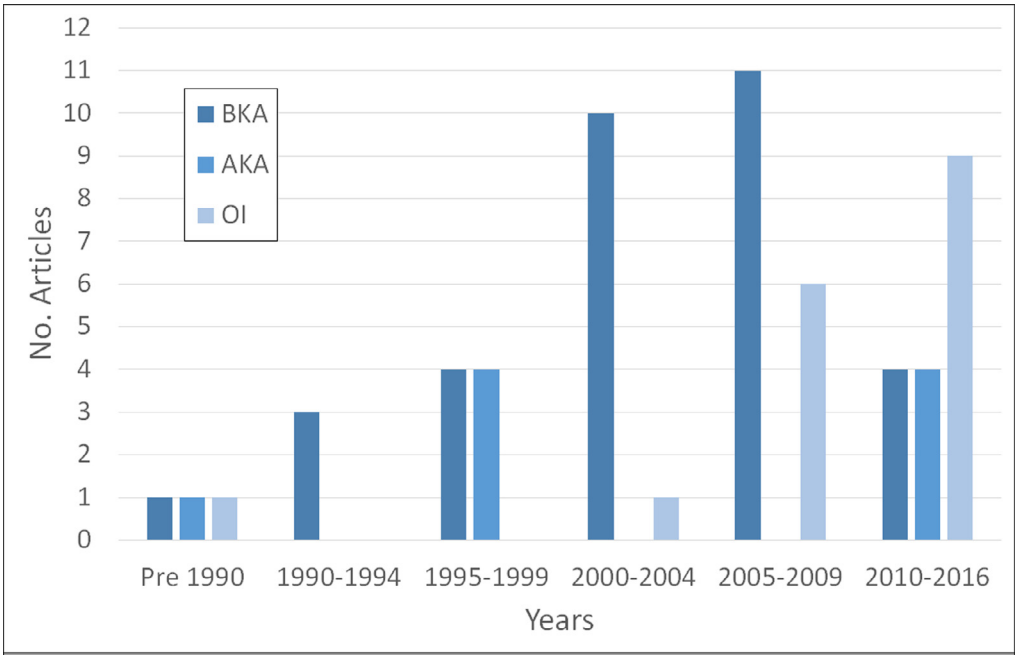


**Fig. 3.** Articles and publication years sorted by intervention. BKA (below knee amputation); AKA (above knee amputation); OI (osseointegrated prosthesis).

## 4. Discussion

### 4.1. Modeling residuum-liner and socket interfaces

The first group of articles studied residual limb–prosthesis interface mechanics (Table 1). Of these, the first seven (published 2000–2005) concentrated upon below knee amputation, and the last three (published 2011–2015) on above knee amputation. Lacroix and Fernandez Patiño 2011 [51] also studied the internal mechanics of the soft tissues.

The residuum–prosthesis interface was the focus of the first substantial effort in computational prosthetic biomechanics research. As a result of the clear importance of this interface, described in the Introduction, sustained work following Krouskop et al's 1987 study [71] has investigated numerically predicted interface stress as a tool to assist in prosthetic socket design (see Section 4.4). The earliest identified studies employed static loading conditions, and assumed rigid bone or prosthetic socket components in single anatomic cases. Particular contributions made by the cited subsequent studies include the generation of all anatomic geometry from single imaging modalities, model loading and boundary conditions incorporating both pre-stresses from socket donning [32] and quasi-dynamic loading [34,36,51], the employment of soft tissue material models capable of demonstrating nonlinear hyperelasticity [51,53], and the assessment of inter-subject variability by simulating multiple cases [51,54]. Prosthetic sockets have generally been represented as a rigid boundary condition, with the argument that the socket has negligible flexibility compared to the soft tissues. Comparison between the rigid-socket BKA studies and the two papers which *did* model the socket [27,32] suggests that this assumption caused an elevation in interface stresses, although the effect is confounded by several factors, most notably the effects of compliant socket liners. It is argued that with present computational power, the various prosthesis socket and liner layers should all be included with representative stiffness.

Interface modeling yields limb–prosthesis pressure and shear stress outputs, which are attractive results because they relate to potentially measurable quantities, assisting model validation. These two topics formed the remit of the 1996 review by Zachariah and Sanders [19], and are updated in Section 5.4.

The choice of contact model will have a substantial influence upon limb–prosthesis interface simulations. Studies identified in the present review addressed the issues associated with large relative tangential displacements by considering contact element types that differ in their contact partner identification technique [27], and by use of explicit finite element formulations [51]. However, within the identified studies, little was reported concerning the friction model itself. Generally, a single coefficient of friction (COF) value was quoted, between 0 (frictionless) and 1 (bonded), but most commonly between 0.4 and 0.5. This indicates the use of a Coulomb 'stick-slip' friction model, whereby tangential force can be transmitted (stick) until its magnitude exceeds the product of the normal force and COF, when tangential relative displacement is permitted (slip). In the cited quasi-static, implicit FE models, it appears that no difference between static and dynamic friction coefficient has been considered. The majority of the cited studies refer to two experimental COF reports: Sanders et al. [72] performed static COF measurements between skin, socks, and conventional socket and liner materials, and Zhang and Mak [73] performed similar dynamic COF measurements. Necessarily, both studies cleaned the test-site skin of their participants, and conducted testing dry, at ambient temperature. Future models may consider the effects of elevated temperature and humidity, and the presence of moisture, grease or sweat at the skin surface, which have been found to have highly variable effects upon COF as reviewed by Derler and Gerhardt [74]. Most recently, Ramirez et al. [75] observed that artificial sweat and hair could produce COF values as low as 0.22, possibly by inhibiting adhesion of stratum corneum cells to the surface [72]. However, the content and quantity of surface moisture are important, and the interpretation of such models must be undertaken with care. Although sweat and sebum may, in sufficient quantities, produce lubricating effects and reduce the shear stress established in the skin, they may also reduce the threshold strains sustainable before tissue damage occurs [76].

**Table 1**
Characteristics of residuum-prosthesis interface mechanics models.

| General | | | Geometry | | Loading | Material Properties | | | | | Prosthesis – Limb Interface | Output: at Prosthesis – Limb Interface |
|---|---|---|---|---|---|---|---|---|---|---|---|---|
| Reference | Objective | Model | Source | n | Scenario | Bone | Soft Tissue | Liner | Socket | Shank | | |
| Zhang and Roberts 2000 [26] | Comparison of FE predicted and experimental pressures and shear stresses. Validated with triaxial force sensors, 8 sites. | BKA, PTB Socket | 3D, Soft Tissue: Digitised limb Bone: biplanar xrays | 1 | PTB rectified socket; Static 800 N axial load | All isotropic and linear elastic | | | | | Friction, μ=0.5 | Pressure: Max 90 kPa at patellar tendon; Shear stress: Max 50 kPa at lateral tibia |
| | | | | | | E=15 GPa $\nu$ =0.3 | E=160-260 kPa $\nu$ =0.49 | E=380 kPa $\nu$ =0.3 | Rigid | N/A | | |
| Zachariah and Sanders 2000 [27] | Comparison of two contact element types on interface stress predictions; sensitivity to interface friction | BKA | 3D, Soft Tissue: Digitised limb Bone: CT of matched pt. | 1 | Static 800 N axial load | All isotropic and linear elastic | | | | | Bonded, Friction, μ=0.675 Frictionless | Pressure: Max (auto friction case) 201.5 kPa; Shear stress: Max (auto friction case) 33.2 kPa |
| | | | | | | Rigid | E=965 kPa $\nu$ =0.45 | N/A | E=1 GPa $\nu$ =0.35 | E=69 GPa $\nu$ =0.3 | | |
| Wu et al 2003 [30] | Proposing socket design guidelines employing FEA, interface pressure and pain-pressure tolerance. Validated with force sensing resistance sensors, pressure at 5 sites. | BKA, KBM vs TSB Sockets | 3D, Unloaded CT of limb in socket | 1 | Static: 235 N axial load (two leg stance), and 470 N axial load (single leg stance) | E=15.5 GPa $\nu$ =0.28 | E=100-400kPa $\nu$ R=0.49 | 5mm thick E=1000 kPa $\nu$ =0.49 | Rigid | N/A | Friction: μ=0.5 (KBM) and μ=0.6 (TSB) | Pressure: Max 250 kPa at lateral tibia (KBM) and 240 kPa at residuum tip (TSB); Shear stress: Max 130 kPa at lateral tibia (KBM) and 60 kPa at residuum tip (TSB). |
| Lin et al 2004 [31] | Influence of liner stiffness on interface pressure and sliding; experimental validation | BKA, KBM Socket | 〃 | 〃 | Static 600 N axial load (single leg stance) | All isotropic, regional-homogeneous, linear elastic | | | | | Friction, μ=0.5 | Pressure: Max 783 kPa; Shear stress: Max 373 kPa; Axial bone – socket slide Max 21.3 mm. |
| | | | | | | E=15.5 GPa $\nu$ =0.28 | E=60-2490kPa $\nu$ =0.45 | 6mm thick E=400-800 kPa $\nu$ =0.45 | Rigid | N/A | | |
| Lee et al 2004 [32] | Influence of pre-stress from socket rectification upon interface stresses | BKA, PTB socket | 3D, Unloaded MR of limb in cast; CAD rectified socket. | 1 | PTB rectified socket; 3 quasi-static knee force and moment sets from inverse dynamics (heel strike, mid-stance, toe-off). | All isotropic, homogeneous, linear elastic | | | | | Friction, μ=0.5 | Pressure: Max 185 kPa, at mid patellar tendon; Shear stress: Max 67 kPa at mid-patellar tendon |
| | | | | | | E=10 GPa $\nu$ =0.3 | E=200 kPa $\nu$ =0.49 | N/A | 4mm thick E=1.5 GPa $\nu$ =0.3[a] | N/A | | |
| Jia et al 2004 [34] | Influence of inertial loads on interface pressure and shear stresses | BKA, PTB socket | 3D, Unloaded MR of limb in cast; CAD rectified socket. | 1 | PTB rectified socket (fixed deflections); quasi-dynamic knee force and moment points in gait cycle from inverse dynamics | All isotropic, homogeneous, linear elastic | | | | | Friction, μ=0.5 | Pressure: Max ~340 kPa, at popliteal depression; Shear stress: Max ~85 kPa at lateral tibia |
| | | | | | | E=10 GPa $\nu$ =0.3 | E=200 kPa $\nu$ =0.49 | E=380kPa $\nu$ =0.39 | Rigid | N/A | | |
| Jia et al 2005 [36] | Influence of inertial loads and gross knee joint displacements on interface pressure and shear stresses | 〃 | 〃 | 〃 | As above, plus knee flexion displacements from kinematic data | All isotropic, homogeneous, linear elastic | | | | | 〃 | Pressure: Max 323 kPa, at popliteal depression |
| | | | | | | 〃 | 〃 | 4mm thick E=380kPa $\nu$ =0.39 | 〃 | 〃 | | |
| Lacroix and Fernandez Patiño 2011 [51] | Explicit (time dependent) model of pre-stress from socket donning process | AKA | 3D, socket from scan of rectified cast, soft tissue and bone from CT | 5 | Socket donned axially along residuum at 6-9mm/s velocity | E=15 GPa $\nu$ =0.3 | 3-parameter hyperelastic, (Mooney Rivlin) $C_{10}$=4.25 kPa, $C_{11}$=0 kPa, $D_1$=2.36 $MPa^{-1}$ | N/A | E=1.5 GPa $\nu$ =0.3 | N/A | Friction, μ=0.415 | Pressure: Max 1.54 – 5.61 kPa; Circumferential shear: Max -0.23 – -0.93 kPa Longitudinal shear: Max -2.00 – 1.99 kPa |
| Zhang et al 2013 [53] | Prediction of AKA socket-limb interface pressure and shear stresses | AKA | 3D, CT for bone and soft tissue. | 1 | 50N axial socket pre-loading; 3 quasi-static knee force and moment sets (heel strike, mid-stance, toe-off). | E=15 GPa $\nu$ =0.3 | 2-parameter hyperelastic (Mooney-Rivlin) $C_{10}$=85.5 kPa, $C_{01}$=21.4 kPa $\nu$ =0.459 | N/A | E=15 GPa $\nu$ =0.3 | N/A | Friction, μ=0.5 | Pressure: Max 119 kPa at ischial bearing area; Shear stress: Max 25.7 kPa longitudinal and 104 kPa circumferential, at brim. |
| Velez Zea et al 2015 [54] | Evaluation of relationship between residuum length and socket-limb interface stress. | AKA | 3D, 'socket' and soft tissue from scans of residuum cast, loaded and unloaded, and bone from CT | 5 | 1) socket pre-loading, 2) relaxation, and 3) stance loading Patient specific load, from static analysis. | E=15 GPa $\nu$ =0.3 | E=2 x$10^{-7}$ GPa[b] $\nu$ =0.475 | N/A | E=1.5 GPa $\nu$ =0.3 | N/A | Friction, μ=0.415 | Pressure: Max 81.7 - 151 kPa, at brim; Shear stress: Max 14.0 – 55.5 kPa. A trend for lower stresses with a longer residuum. |

KEY: 〃 = ditto, as in same-group study listed above; AKA = above knee amputation; BKA = below knee amputation; CT = computed tomography imaging; E = Young's modulus; KBM = Kondylen Betrung Munster BKA socket design; MR = magnetic resonance imaging; n = number of patients or geometries; N/A = not applicable; N/S = not stated; $\nu$ = Poisson's ratio; PTB = patella tendon bearing BKA socket rectification; TSB = total surface bearing BKA socket design; μ = coefficient of friction.

[a] A finite socket material stiffness was reported, but exterior of socket was constrained against motion, so socket flexibility effects would be negated; [b] believed to mean 2x$10^{-4}$ GPa, or 200 kPa

### 4.2. Residuum soft tissue internal mechanics

It is now understood that pressure ulcers can develop in deep tissue adjacent to bony prominences, and may only display external signs of injury after extensive tissue damage has occurred [77]. Tissue damage may result from compression-induced ischaemia, and shear strain above a threshold level [78]. This is of particular concern in the reconstructed soft tissue pad in the amputated limb, especially early in rehabilitation, due to the combined action of cyclic and sustained compressive and shear loads and elevated temperatures experienced in tissues which are not used to load-bearing.

#### 4.2.1. Developments in residuum internal soft tissue modeling

The primary modeling focus shifted from residuum–prosthesis interface mechanics to the internal mechanics of the soft tissues (Table 2), since approximately 2006, with notable efforts from Portnoy in Gefen's group at Tel Aviv University [43–46, 49]. Again the focus was initially on below-knee amputation, and particular contributions include the improvement of model geometry and material model definitions, and the use of Open MR (magnetic resonance) imaging to characterize 3D tissue displacements under load. Two later papers considered the above-knee case [51,52], with Lacroix and Fernandez-Patiño introducing explicit FEA formulation to simulate the large-displacement sliding scenario of socket donning. Sanders and Daly [79] reported in 1993 the interface shear stresses generated by ambulation loading, and the important element introduced by Lacroix and Fernandez-Patiño's study was the explicit simulation of socket donning, which enabled additional residual shear stress to be captured. Earlier models simulated the tissue–socket interference fit by imposing 'overclosure' displacement normal to the surface, and were thus only capable of generating interface compression. These are both valuable contributions to the prediction of combined interface pressure and shear stress distributions, as well as the deviatory and dilatational components of soft tissue strain. These factors will have considerable

**Table 2**
Characteristics of residuum soft tissue mechanics models.

| General | | | Geometry | | Loading | Material Properties | | | | Prosthesis – Limb Interface | Output (all in Soft Tissue) |
|---|---|---|---|---|---|---|---|---|---|---|---|
| Reference | Objective | Model | Source | n | Scenario | Bone | Soft Tissue | | Socket | | |
| Portnoy et al 2007 [43] | Developing and validating a real-time tissue stress predictor from xray measurements and limb-socket interface loads. | BKA | 2D Plane Strain, parametric from xray | 5 | Quasi-static limb-socket interface loads from 7 Tekscan force sensors, in gait. | All isotropic, homogeneous, linear elastic | | | | Friction, μ=0.5 | von Mises stresses, and compressive Principal stresses along fibular and gastrocnemius 'axes'. |
| | | | | | | Rigid | $\nu$ =0.49 | | N/A | | |
| | | | Phantom 3D: Visible Human Project | 1 | Static 400 N axial force on knee | E=7.3 GPa $\nu$ =0.3 | E=100 kPa $\nu$ =0.49 | | Rigid | | |
| Portnoy et al 2008 [44] | Characterising the mechanical conditions in muscle flap after donning socket and with load bearing.<br>Interface stress validation by two thin film pressure sensors, with 150-175 locations and approx. 1mm spatial resolution. | BKA | 3D, Open MR. Unrectified cast used as socket. | 1 | Static, 0.9 mm axial displacement of residual bones from end loading in Open MR scanner. Validated with limb-socket interface pressures. | Rigid | Muscle: neo-Hookean, $G^{ins}$=8.5 kPa, Viscoelasticity from Prony series expansion | Skin: Incompressible, 2-parameter hyperelastic, $C_{10}$=9.4 kPa, $C_{11}$=82 kPa | E=1 GPa $\nu$ =0.3 | Friction, μ=0.7 | Strain energy density (max 104 kJ/m$^3$);<br>Principal tensile strain (max 129%);<br>Principal compressive strain (max 85%);<br>Maximal shear strain (max 106%);<br>Principal tensile stress (max 263 kPa);<br>Principal compressive stress (max 240 kPa);<br>Maximal shear stress (max 23 kPa);<br>von Mises stress (max 215 kPa). |
| Portnoy et al 2009a [45] | As above, considering model variants to assess the effects of risk factors: bone fragment shapes, scarring, and muscle properties. | BKA | " | " | " | " | Homogeneous, isotropic, 3-parameter hyperelastic, (generalised Mooney Rivlin) function. | | | " | " | " |
| | | | | | | | Muscle: $C_{10}$=2.3-8.1 kPa, $C_{11}$=0 kPa $D_1$=4.4-1.2 MPa$^{-1}$ | Fat: $C_{10}$=0.143 kPa, $C_{11}$=0 kPa $D_1$=70.2 MPa$^{-1}$ | Skin (2mm): $C_{10}$=9.4 kPa, $C_{11}$=82 kPa $D_1$=0 MPa$^{-1}$ | | |
| | | | | | | | Single parameter ($C_{10}$=148.9 kPa) scar model. | | | | |
| Portnoy et al 2009b [46] | Characterising the mechanical conditions in muscle flap in multiple patients, assessing variability, and DTI risk through muscle injury threshold strain/time. | BKA | " | 5 | Static, patient specific axial displacement of residual bones extracted from end loading in Open MR scanner. | " | Muscle, Fat and uniform 2mm Skin regions. Generalised 3-parameter hyperelastic (Mooney-Rivlin) function. Constitutive parameters not specified: displacement-strain analysis only. | | | " | " | Principal compressive strain (mean 3.1-15.5%), Principal tensile strain (mean 2.8-13.7%), and maximal shear strain (mean 2.9-14.9%). |
| Portnoy et al 2011 [49] | Characterising the mechanical conditions in muscle flap whilst seated, and DTI risk through adaptive stiffening muscle injury simulation. | BKA | " | 1 | Seating. Measured limb-socket interface pressures applied to soft tissue. | " | Homogeneous, isotropic, 3-parameter hyperelastic, (generalised Mooney Rivlin) function. | | | N/A | N/A | Principal compressive stress (max 102 kPa), Principal tensile stress (max 66.6 kPa), von Mises stress (max 129 kPa), max. shear stress (max 67.2 kPa), injury rate (max 8.67 mm$^3$/min). |
| | | | | | | | Muscle: $C_{10}$=4.25 kPa, $C_{11}$=0 kPa $D_1$=24.34 MPa$^{-1}$ | Fat: $C_{10}$=2.97 kPa, $C_{11}$=0 kPa $D_1$=34.8 MPa$^{-1}$ | Skin (1mm): $C_{10}$=9.4 kPa, $C_{11}$=82 kPa $D_1$=0 MPa$^{-1}$ | | |
| Lacroix and Fernandez Patiño 2011 [51] | Explicit (time dependent) model of pre-stress from socket donning process | AKA | 3D, socket from scan of rectified cast, soft tissue and bone from CT | 5 | Socket donned axially along residuum at 6-9mm/s velocity | E=15 GPa $\nu$ =0.3 | Homogeneous, isotropic, 3-parameter hyperelastic, (generalised Mooney Rivlin) function. $C_{10}$=4.25 kPa, $C_{11}$=0 kPa, $D_1$=2.36 MPa$^{-1}$ | | E=1.5 GPa $\nu$ =0.3 | Friction, μ=0.415 | Principal compressive strain (max 31-74%), Principal tensile strain (max 18-64%), von Mises stress (max 5-24 kPa). |
| Ramírez and Vélez 2012 [52] | Influence of bone-soft tissue contact condition: friction (μ=0.3) and fully bonded. | AKA | 3D, socket and soft tissue from laser scans, bone from CT. | 4 | Socket pre-loading, Quasi-static two-leg stance (50% bodyweight). | E=15 GPa $\nu$ =0.3 | E=200 kPa $\nu$ =0.475 | | E=1.5 GPa $\nu$ =0.3 | Friction, μ=0.415 | Principal compressive strain: (max 85-163%); Principal tensile strain: (max 26-118%); von Mises stress: (max 120-860 kPa)[a]. |

KEY: " = ditto, as in same-group study listed above; AKA = above knee amputation; BKA = below knee amputation; $C_{10}$ and $C_{11}$ = Mooney Rivlin hyperelasticity constitutive model parameters; $D_1$ = Mooney Rivlin compressibility constitutive model parameter (incompressible if unity); DTI = deep tissue injury; E = Young's modulus; $G^{ins}$= transverse shear modulus of muscle in neo-Hookean model; MR = magnetic resonance imaging; n = number of patients or geometries; N/A = not applicable; N/S = not stated; $\nu$ = Poisson's ratio; μ = coefficient of friction.

[a] The highest peak stresses were possibly associated with a stress concentration near a model boundary condition.

influence upon the prediction of injury risk, discussed further below.

Considering the developments in applied material models for the soft tissue structures, linear elastic simplifications have been largely replaced by models which allow hyperelasticity and, in one case, viscoelasticity, although maintaining assumptions of isotropy and within-tissue homogeneity.

The majority of the identified studies considered relatively conventional modeling output measures including maximum and minimum principal stresses and/or strains, strain energy density, and equivalent stress magnitude (commonly referred to as 'von Mises' stress in FEA packages). Another interesting contribution of Portnoy et al. in their 2011 paper [49] related to their model post-processing using two phenomenological deep tissue injury (DTI) rules. First, employing principles developed by Linder-Ganz et al. [80], they considered a sigmoid pressure–time threshold for muscle tissue injury based upon compressive stress:

$$\sigma = \frac{K}{1 + e^{\alpha(t - t_0)}} + C \quad (1)$$

where $\sigma$ is a compressive Cauchy stress, $t$ is the exposure time, and $K$, $\alpha$, $t_0$ and $C$ are empirical constants from animal data. This technique was extended two years later by Gefen et al, in terms of strain [15].

Second, the study used this prediction of the cause of tissue injury to predict its progression, by implementing a time-based stiffening of damaged tissue material properties through iterative FE solutions as follows:

$$G^{injured} = G^{uninjured}(A_0 + A_1\sigma + A_2 t) \quad (2)$$

where $G^{injured}$ and $G^{uninjured}$ are the muscle tissue shear modulus values, and $A_0$, $A_1$ and $A_2$ are empirical constants again from animal data [81]. Thus, the progressive risk of DTI could be predicted around bony prominences in the residual limb.

#### 4.2.2. Tissue nonlinear elasticity/hyperelasticity

Linear elasticity was assumed for the soft tissue models in the earlier studies identified in this review (Table 3, 2000–2007). This is appropriate for materials that deform and recover in a linear manner in response to applied load, and according to Hooke's law

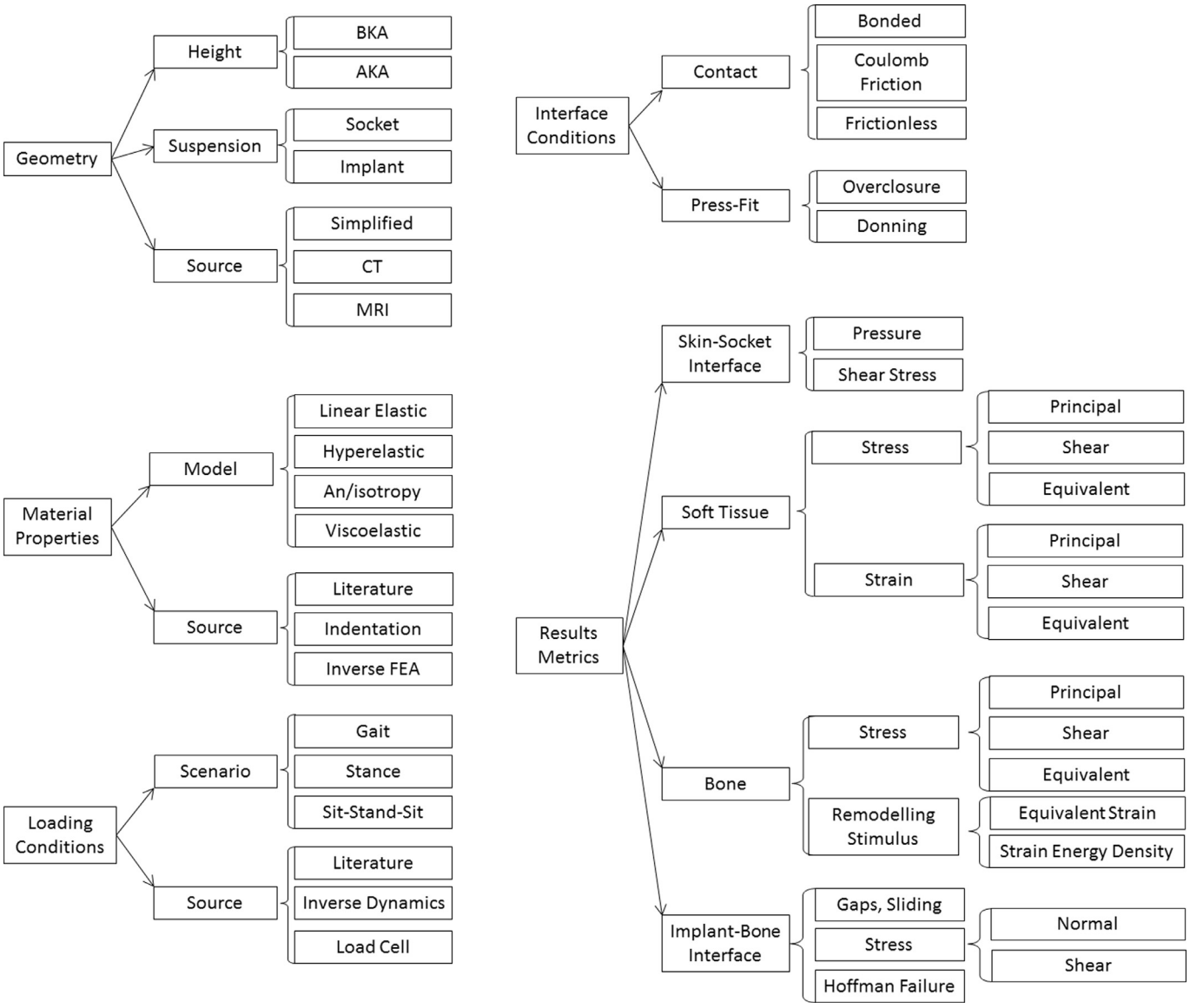


**Fig. 4.** Methodological and results categories extracted from the identified studies, grouped by analysis input (pre-processing) and output (post-processing) parameters.

**Table 3**
Employed soft tissue elasticity models (see also Appendix).

| Formulation | SED Function $W$ | Uses in reviewed studies | Constitutive model parameters | Source | Species/Site |
|---|---|---|---|---|---|
| Neo-Hookean | $W = \frac{G}{2}(I_1 - 3) = C_{10}(I_1 - 3)$ | Muscle [44] | $G$ = 8.5 kPa | [91] | Porcine, Gluteus |
| | | Scar [45] | $C_{10}$ = 148.9 kPa | [175] | Human, Skin (Burn) |
| Neo-Hookean, Compressible | $W = C_{10}(I_1 - 3) + \frac{1}{D_1}(J-1)^2$ | Fat [45] | $C_{10}$ = 0.143 kPa, $D_1$ = 70.2 MPa$^{-1}$ | [176] | Ovine, over Gluteus |
| | | Fat [49] | $C_{10}$ = 2.97 kPa, $D_1$ = 34.775 MPa$^{-1}$ | [177] | Human, Breast |
| | | Muscle [45] | Soft, Flaccid $C_{10}$ = 2.3 kPa, $D_1$ = 4.36 MPa$^{-1}$ | [91] | Porcine, Gluteus |
| | | Muscle [49] | Ave, Flaccid $C_{10}$ = 4.25 kPa, $D_1$ = 2.36 MPa$^{-1}$ | [91] | Porcine, Gluteus |
| | | All soft tissue [51] | Stiff, Flaccid $C_{10}$ = 6.2 kPa, $D_1$ = 1.62 MPa$^{-1}$ | [91] | Porcine, Gluteus |
| | | | Contracted $C_{10}$ = 8.075 kPa, $D_1$ = 1.243 MPa$^{-1}$ | [178] | Human, Rectus Femoris |
| | | | $C_{10}$ = 4.25 kPa, $D_1$ = 24.34 MPa$^{-1}$ as Ave, Flaccid Muscle in [45] | [91] | Porcine, Gluteus |
| Mooney Rivlin | $W = C_{10}(I_1 - 3) + C_{01}(I_2 - 3)$ | All soft tissue [53]* | $C_{10}$ = 85.5 kPa, $C_{01}$ = 21.38 kPa | [179] | Human, Plantar |
| Extended Mooney | $W = C_{10}(I_1 - 3) + C_{11}(I_1 - 3)(I_2 - 3)$ | Skin [44,45,49] | $C_{10}$ = 9.4 kPa, $C_{11}$ = 82 kPa | [82] | Human, Volar Forearm |

KEY: $C_{ij}$ = deformation constitutive model parameter (material property); $D_1$ = volumetric constitutive model parameter; $G$ = shear modulus; $I_1, I_2$ = invariants of principal stretch ratios; $J$ = total volume ratio; $W$ = strain energy density.

* compressibility was included by stating a Poisson's ratio, which ABAQUS uses as $D_1 = \frac{3(1-2\nu)}{2(C_{10}+C_{01})(1+\nu)}$.

this behavior can be characterized for infinitesimal strains by the Young's modulus ($E$) and the Poisson's ratio ($-1 \leq \nu \leq 0.5$) alone. The Poisson's ratio, the ratio of transverse to axial strain, is related to the material's compressibility. Soft tissues are commonly considered incompressible ($\nu = 0.5$) owing to their high water content, although this limiting value can produce numerical singularities in the FEA computation, so values of $\nu = 0.45 - 0.49$ were used by the earlier studies identified in this review. They also, however, commonly exhibit large strains and non-linear stress–strain behavior. In their 2003 indentation test and FEA study (discussed in more detail below), Tönük and Silver-Thorn [29] used a hyperelastic soft tissue model. Portnoy et al's 2008 paper [44] introduced this in a full residuum–socket model. Across the variety of sources consulted, a range of different notations have been used so the application of hyperelastic models is reproduced in Appendix, employing notation in general from Portnoy et al's work and ABAQUS, the most commonly employed finite element solver in the cited studies, for clarity.

Several hyperelasticity models have been employed in modeling the soft tissues in amputated limbs, which are formed from a strain energy density (SED) function $W$. This is expressed in terms of the deformation invariants of principal stretch ratios $I_1$ and $I_2$, and the total volume ratio $J$, which are calculated from the FEA-predicted model deformations. The SED function contains constitutive parameters $C_{ij}$ and $D_1$ which are material constants, and these are obtained by empirical fit of a selected SED function's stress–strain profile to experimental data [82]. The identified studies used SED functions taken from general material characterization studies rather than model or patient-specific information. Furthermore, by necessity several of these past studies used ex-vivo animal tissue for characterization.

The identified studies employing linear elastic material models for all soft tissue, generally those investigating limb surface stresses only, eventually followed Zhang et al's 1995 [83] model of $E = 200$ kPa, $\nu = 0.49$. The later identified studies, mainly those investigating internal soft tissue stresses, employed hyperelasticity (Table 3). The established approach, which has informed the majority of successive studies, was presented in Portnoy et al's 2009 residuum risk factor parameter study [45]. This used compressible Neo-Hookean models for fat and muscle, varied for several levels of stiffness and contraction, an incompressible Neo-Hookean model for scar tissue, and an incompressible extended Mooney model for skin.

A general observation across the models reported in Table 1 and Table 2 is that peak predicted limb–socket interface normal stresses under stance and gait loading were markedly higher in earlier studies. This is attributed to the earlier use of linear elastic soft tissue models (typical peak normal stresses of 200–350 kPa) with larger elastic moduli than when hyperelasticity was introduced (typically 120–260 kPa). As noted, peak internal strain is currently preferred to surface stresses in predicting tissue damage [15], so appropriate elasticity models and consideration of pre-strain from socket donning are essential.

#### 4.2.3. Residuum thermal analysis

Finally, to return to the systematic review-identified studies, one paper was identified that conducted particularly notable internal tissue analysis in the residuum. Peery et al. [84] considered the thermal conditions in the residual limb tissues after donning a socket, and validated their models against experimental surface temperature measurements at rest. Such simulations are of future value in parallel with structural analysis, to evaluate the combined influence of mechanical deformations and elevated temperature or humidity upon the risk of tissue damage. Indeed elevated temperatures have a detrimental effect on skin by affecting its mechanical stiffness and strength [85], therefore increasing the risk of tissue damage [86]. Elevated moisture will also soften skin and increase cellular permeability leading to a greater susceptibility to skin irritation [87]. In some scenarios, moist skin will also have an increased coefficient of friction, resulting in elevated shear forces at the device-skin interface [88].

### 4.3. Identification of residuum tissue characteristics

#### 4.3.1. Soft tissue model constitutive parameters

A third set of identified studies employed FEA to determine residuum soft tissue characteristics, making notable contributions of material models for nonlinear elasticity and viscoelasticity effects, representing an improvement in model fidelity. The authors inferred the soft tissues' material properties from experimental data using the empirical, iterative 'inverse method'. In 2003, Tönük and Silver-Thorn [29] reported soft tissue indentation tests on 7 patients, and then produced axisymmetric indentation FE models in order to identify regionally appropriate nonlinear elastic constitutive coefficients for a simplified 3-parameter James-Green-Simpson strain energy density function (see Appendix). Models were patient-specific, representing 11 locations of interest in socket rectification, with dimensions taken from magnetic resonance (MR) imaging or x-ray computed tomography (CT) scans. The models were solved with iterative modifications to the constitutive model coefficients at three displacement rates until less than 1% normalized sum of square error (NSSE) was obtained between experimental and numerical indenter forces. Coefficients were found to vary substantially between individuals and sites, and within-individual for a particular tissue site after a 20-month period. Their parameter search method was structured but manual, so may have identified local NSSE minima, which may be avoided using more automated minimization methods, or Monte Carlo approaches [89]. They extended this work to include viscoelastic effects in 2004 [33], described below.

More recently researchers at MIT published further work towards the same goal, including a robotic limb indentation device which builds a map of tissue compliance at 18 locations. This was used with inverse FEA to identify constitutive parameters of a 2nd order Ogden hyperelastic material model, incorporating viscoelasticity, by optimization [50]. It is difficult to assess the agreement between the tissue property predictions obtained from these studies due to the different material models employed. Furthermore, high variability was reported between individuals [29,33], and marked spatial and temporal variation was observed in the properties calculated for the same individual.

#### 4.3.2. Time dependent soft tissue properties

Time dependency of soft tissue loading in residuum FE models has received relatively little attention, although several of the experimental material property reports cited in Table 3 do present applicable data. A small subset of studies have attempted to incorporate the viscoelastic process of stress relaxation (whereby under a constant, finite strain, stress decreases), and one considered creep (where strain increases under a constant, finite stress).

Portnoy et al's 2008 paper [44] reported the use of stress predictions to infer the risk of soft tissue injury. These authors applied a Prony series expansion to represent stress relaxation [90]. The asymptotic relaxation level was defined in terms of the shear modulus at the instant of load application $G^{ins}$ and after relaxation $G^{\infty}$ by:

$$\delta = \frac{\left(G^{ins} - G^{\infty}\right)}{G^{ins}} \tag{3}$$

They modified $S$, the second Piola – Kirchhoff stress from the FE database, by the Prony method:

$$S \cong (1-\delta)\frac{\partial W}{\partial E} + \int_0^t \delta \frac{\partial W}{\partial E} e^{-(t-\xi)/\tau} d\xi \quad (4)$$

where $E$ is the Green Lagrange strain, $\delta$ is the magnitude relaxation parameter, the percentage difference between tissue moduli at the instant of strain initiation and after relaxation, and $\tau$ is the time constant of relaxation. They did not model the stress relaxation transient, as they were considering long-term deep tissue injury (DTI), and so simplified their asymptotic stress level to:

$$S \cong (1-\delta)\frac{\partial W}{\partial E} \quad (5)$$

where $\delta$ was taken as 0.5 [91].

Obtaining the temporal parameters of the viscoelastic relaxation function would potentially enable researchers to represent the transient effects of stress relaxation explicitly.

Tönük and Silver-Thorn [33] used their previously reported time-independent model with a Prony series expansion and a linear Kelvin–Voigt model of viscoelasticity. They used regression between experimental and simulated indentation to fit both hyperelastic constitutive model parameters, and magnitude and temporal viscoelasticity parameters. They also considered both short and long term viscoelastic effects, and indenter force relaxation and creep data for step displacement and force responses, respectively. They noted that different viscoelastic parameters were obtained when creep and relaxation data were used. Alongside expected variations from model simplifications and experimental error, the creep and relaxation data were collected on different days, suggesting appreciable diurnal variation in tissue behavior. Sengeh et al. employed a related approach in their robotic indenter residual limb tissue compliance mapping study [50], using the two constitutive parameters of their Ogden hyperelastic model and a two-parameter viscoelastic relaxation function, and found less spatial variability in calculated properties for their test participant than Tönük and Silver-Thorn observed in their group.

Tönük and Silver-Thorn [33] acknowledged that the applied material models can only offer phenomenological representation of the underlying physiological processes which produce time-varying properties, and as noted above, different methodologies precludes comparison of the results obtained in the small number of studies in this area. There is still a need for systematic evaluation of the temporal changes in soft tissue behavior and inter-subject variability, and potential value in comparison of different nonlinear elastic constitutive models.

#### 4.3.3. Pressure-pain tolerance thresholds

With an alternative approach, in 2005 Lee, et al. [37] used a simplified FE model of indentation in a single individual, and physical tests from 11 locations in 8 individuals, to investigate relationships between pain threshold and tolerance with indenter pressure and tissue distortion. This was conducted at below-knee residual limb locations with a range of soft tissue layer thicknesses, and for a range of subject ages, and three linear elastic soft tissue models from literature data. Local differences in pain tolerance and threshold pressure levels were observed, with highest values as expected at the mid-patellar tendon and tibial tuberosity, and lowest values at the residuum tip. Like the studies discussed above, the authors demonstrated the importance of collecting personalized data: significantly higher average pain tolerance and threshold pressures were recorded for the two youngest individuals in the study. Two years later Lee and Zhang proposed the application this technique as part of a simulation-aided socket fitting process [42], one of the long established goals of numerical simulation of the amputated lower limb, discussed below.

### 4.4. Proposals for incorporating FEA into prosthesis fitting and socket fit assessment

The first proposals for incorporating numerical predictions into the CAD/CAM-based prosthesis fitting approach were made in the 1980s by researchers in Texas [71] and University College London [92]. Five relevant papers were identified in this area in the present review.

The first key contribution to FEA-informed socket design incorporated person-specific, comfort-based design parameters. Wu et al. [30], and Lee and Zhang [42] both used indenter systems to characterize the local surface pressure-pain tolerance (PPT) of a single patient. As an assessment of goodness-of-fit, they then compared the PPT to FE-predicted socket contact pressures to assess the risk of discomfort. While Wu et al. assessed a socket fabricated before the study, Lee and Zhang demonstrated how the prediction of PPT could be used as feedback to guide the socket design.

Amali et al. attempted to simplify the use of FEA in socket design or pre-clinical analysis [28]. They advocated analyzing limb–socket interface stress data from FEA predictions or physical measurements using Artificial Neural Networks (ANN) in order to produce a transfer function to simplify the response to changes in complex input parameters, such as patient and prosthesis geometry and material properties. This study contributes an important proposal to reduce the computational time and expertise requirements that are likely to present barriers to clinical adoption of FEA.

To a similar goal, Portnoy et al. proposed a subject-specific method for real time DTI risk evaluation [47]. A portable monitor was developed to measure the contact force between the residuum and the prosthetic socket at the distal tip of the residual tibia. A set of equations was used to predict the soft tissue stress in this location based upon this force, measurements of the individual's anatomy from radiographs, and soft tissue material properties, which were validated against an axisymmetric FE model. The equations were used to calculate real-time subject-specific internal stresses and stress-time integrals for a range of walking surfaces and slopes, which were compared to a muscle cell death threshold level [80]. As well as computational efficiency, this study represents a notable contribution as it takes a more physiology-based approach to the socket fit design parameter definition than pressure-pain tolerance. This is likely to be safer especially for individuals experiencing diminished sensation, but relies on the collection of appropriate and specific tissue injury threshold data.

Goh et al. demonstrated how their in-house FE code could be directly integrated with a commercial CAD software package [38], comparing FE predictions with experimental measurements from pressure transducers at 16 sites on the socket. They proposed using FEA-derived interface pressure predictions to iterate socket design, and note the requirement of further work to compare the pressure values to a personalized pain or discomfort measurement, to evaluate goodness-of-fit. Studies by the Colombo group in Milan, summarized in 2010 [48] have extended this idea. A methodology was created to design, virtually test and automatically optimize the socket for an individual patient. The patient's anatomy was characterized using surface laser and MRI scanning, linear material properties for the patient's soft tissue were calculated using indenter data, and iterative socket rectifications were made digitally [93]. More recent research has proposed how the rectification might be performed automatically based on empirical rules [94] which relate the local rectification depth to local qualitative scores of soft tissue tonicity, 'K' activity levels and subject weight. FE modeling techniques were used as a predictor for socket performance, and the definitive socket was manufactured using rapid prototyping techniques. The Milan studies focused on methods such as artificial neural networks for identification of rectification zones, but did not note specific outcome measure targets to predict goodness-of-fit.

Drawing consensus from all these identified studies, it is likely that informed socket design will require patient-specific geometry, material properties and pressure tolerance measurements, all of which may be collected clinically. To go beyond interface pressure and take a pathophysiological approach, modeling should focus on the translation of these loads into the underlying tissues, in the form of how tissues deform under load and the implications for tissue viability. A novel automated design method should then be compared to traditional methods of socket design, to assess the value of the advanced technology and its efficacy.

### 4.5. Analysis of prosthetic componentry concepts

Key examples of prosthetic limb or socket mechanical design considering explicitly the effect upon the residual limb were performed for the 'monolimb' concept. Preclinical analysis investigated the influence of shank stiffness upon residual limb–socket interface stress, considering shank cross section shape vs. interface pressure [35], and shank wall thickness and material vs. interface pressure and shear stress [41]. Modifications to conventional socket designs have also been considered in terms of compliant features and regions of reduced wall thickness aiming to achieve local compliance for pressure relief [39].

Numerical models have some precedence for use in analysis of the prosthetic components. Several past studies have considered the mechanics of prosthetic limb components [95], and novel socket designs [96], but studies which did not also consider the residual limb were excluded from the systematic review raw search results. The boundary conditions provided to a prosthesis model are likely to be more trustworthy where the residual limb is modeled explicitly. However, the studies in this small subset were guided by the state of the art presented in Table 1, and were performed for single residuum shape cases only. For robust preclinical analysis it is important to evaluate a concept's performance across the likely range of patient anatomy and loading conditions, in order to identify worst cases or limits of clinical applicability. Furthermore, a residuum FE model employed in pre-clinical analysis of novel prosthetic concepts must be validated in use with one or more conventional prosthesis designs, especially if the concept in consideration is an extrapolation versus devices in clinical use.

### 4.6. Analysis of osseointegrated prosthesis concepts

As a final main use of numerical models of the amputated lower limb, the concept of osseointegrated prosthetics has received considerable attention since 2000. Developed by Brånemark et al. from dental implant fixation technology [97], osseointegration provides direct anchoring of the prosthetic limb to the residual bone. In treatment of above-knee amputation as with dental implantology, surgery is conventionally a two-stage procedure. First, an implant is placed in the residual femoral canal, the amputation site is closed, and biological fixation is allowed to establish prior to a second procedure. Approximately 6 months later the distal bone tip is exposed again, and a skin-penetrating abutment or coupler is attached [98,99]. Compared to socket suspension, OI prosthesis suspension is argued to improve function, gait motion and quality of life [100], to reduce the number of return visits to prosthetists and potentially the post-surgical rehabilitation cost [3]. Observed complications of OI prosthesis suspension have included early loosening, superficial infection, and occasional deep infection [101]. Bone fractures, mechanical deformation and failure of the implants have been reported [98], and periprosthetic bone remodeling is observed [60].

#### 4.6.1. Developments in modeling the OI implant–bone construct

The first computational biomechanical investigation of osseointegrated implant geometry using numerical modeling was reported by Krouskop et al. in 1976 [102], substantially before the technology was first used to treat lower limb amputation in the 1990s. No other OI-related studies were excluded from the systematic review due to the post-2000 date restriction. The search results showed a marked increase in computational biomechanics activity in this area after 2000, with purely FEA-based biomechanics studies of OI concepts found at approximately one per year from 2005 onwards [55–61,63,66–69] (Table 4). The research approach in this area is similar to studies on arthroplasty prostheses, and long-stemmed cementless total hip implants in particular, concentrating on: (1) implant-bone interface mechanics, with regard to fixation and loosening, (2) bulk bone strain, with regard to periprosthetic fracture, and (3) predicting the stimulus for, and then the progression of periprosthetic bone remodeling. After initial use to drive implant geometry optimization studies [55–57,61], these factors have been compared for different clinically-used implant designs [58,59,63,66], to understand their observed bone response [60,70], and to propose new concepts [67,68]. The cited studies have contributed developments in the range of expected implant–bone load cases, and results parameter interrogation. This has provided enhanced understanding of the short and medium term performance of existing implants, and will enable greater confidence in future preclinical analysis work. These isolated implant-bone construct models have been validated experimentally using cadaver tests and strain gauging [68]. Although not including finite element analysis, and employing a simplified implant support structure, Thompson et al have conducted full-surface experimental strain measurement techniques for assessing OI implant mechanics [103]. These techniques have promise for validation of FE models owing to their data richness compared to discreet strain gauges, with particular value in the comparative pre- and post-implantation bone strain analysis [104] which is used as an analogue of bone remodeling stimulus.

Starting to consider more advanced implant-bone physiology, two additional articles were identified from the Veterans Affairs Department/University of Utah, which employed FEA to investigate the bioelectric conditions in the above-knee amputated limb with the application of electrical stimulation to promote osseointegration [62,64]. The electric field and current density in the residual limb were predicted, generated by the application of a potential difference between the OI prosthesis (cathode) and two skin-surface anodes. This represents an early but important step in bone morphology modeling. These investigations were conducted for eleven individuals displaying a range of extents of heterotopic ossification (HO), a relatively common phenomenon in blast trauma amputation and servicepeople in particular [105]. This was the first study identified in this review to address this highly complex and variable phenomenon by modeling.

#### 4.6.2. Dynamic and abnormal loading conditions

Scope for further purely biomechanical work in this area may be focused upon dynamic and abnormal loading conditions, owing to the substantially changed stresses imposed upon the bone surrounding the implant. The dynamic loads experienced by an OI prosthesis and its fixation to the bone have been studied in detail by Frossard et al. [106] in collaboration with researchers at Sahlgrenska who developed the original OPRA prosthesis. Their results indicated the potential differences in loads and impulses generated in gait using different prosthetic limb componentry, providing valuable input data for dynamic computational models. As noted above, periprosthetic bone fracture, mechanical failure of the implant–bone interface, and of the implant and abutment components themselves, are understood to be some of the main mechan-

**Table 4**
Characteristics of osseointegrated prosthesis concept models.

| General | | | Geometry | | Loading | Material Properties | | | | Implant-Bone Interface | Output |
|---|---|---|---|---|---|---|---|---|---|---|---|
| Reference | Objective | Implant | Source | n | Source | Bone | Implant | | | | |
| | | | | | | | Material | E / GPa | $\nu$ | | |
| Xu et al 2000 [55] | Parametric implant design study: internal and external diameters, length, threads | Generic, parametric, threaded cylindrical design; OPRA-like | Idealised 2D axisymmetric | 1 | Quasi-static knee force and moments from gait | Transversely isotropic, homogeneous | CPTi | 115 | 0.3 | Bonded | von Mises bone stress; bone strain |
| Xu et al 2006 [57] | CT-based modelling method for implant and bone stress analysis | Generic, threaded cylindrical design; OPRA-like | 3D, CT | 1 | ″ | ″ | ″ | ″ | ″ | ″ | ″ |
| Xu et al 2008 [60] | Periprosthetic bone remodelling analysis | OPRA | 3D, CT | 1 | ″ | ″ | ″ | 110 | 0.5 | ″ | von Mises bone strain Principal bone stress |
| Zheng et al 2005 [56] | Analysis of implanted bone stress and change vs. intact case, and retained bone length | Generic, single-part and multi-part design incl. silicon damper | 3D, CT simplified | 1 | Quasi-static force representing heel strike | Isotropic, homogeneous | N/S | 116 | 0.3 | Bonded | von Mises bone stress |
| Lee et al 2007 [58] | Implant-bone interface stress distribution | OPRA | 3D, Sawbone | 1 | Simplified (pure axial); Instrumented prosthesis (triaxial forces and moments). | Isotropic, homogeneous | CPTi | 110 | 0.3 | Bonded | von Mises bone stress |
| Lee et al 2008 [59] | Implant-bone interface stress distribution | ″ | ″ | ″ | As above, plus quasi-static gait cycle loads. | Anisotropic, homogeneous | ″ | 115 | 0.3 | ″ | ″ |
| Helgason et al 2009 [61] | Optimising implant design Periprosthetic bone failure and implant failure risks | 'Optimised' parametric design | 3D, CT | 1 | Gait; set of quasi-static triaxial forces and moments. | Isotropic, inhomogeneous | Ti-6Al-4V | 110 | 0.3 | Frictionless contact or bonded | Bone Risk of Fracture; Implant Risk of Fracture |
| Tomaszewski et al 2010 [63] | Periprosthetic fracture and bone remodelling stimulus | OPRA; ISP Endo/Exo; Intact femur ref. | 3D, CT | 1 | Instrumented prosthesis Heel strike and toe-off load cases | Isotropic, inhomogeneous | OPRA: CPTi | 110 | 0.3 | Friction, μ=0.4; Then Bonded | von Mises bone stress; Strain Energy Density; Hoffman interface failure criterion |
| | | | | | | | ISP: CoCrMo and spongiosa | 210 | 0.3 | | |
| | | | | | | | | 1 | 0.3 | | |
| Tomaszewski et al 2012a [66] | Periprosthetic fracture and adaptive bone remodelling | ″ | ″ | ″ | ″ | ″ | ″ | ″ | ″ | Bonded | von Mises bone stress; Strain Energy Density stimulated density adapting remodelling |
| Tomaszewski et al 2012b [67] | ″ | As above, plus New design concept | ″ | ″ | As above, plus forward fall load case | ″ | As above, plus, for New design: Ti-6Al-4V and PEEK | 114<br>12.5 | 0.3<br>0.4 | ″ | ″ |
| Tomaszewski et al 2013 [68] | Intact and implanted bone strain, and comparison to cadaver tests (n=7) | OPRA; New design concept (Ti-6Al-4V / PEEK) | ″ | ″ | Instrumented prosthesis Heel strike, toe off, and one-leg stance load cases | ″ | ″ | ″ | ″ | ″ | Equivalent stress and strain distributions in implant and bone; Cortical bone strain; |
| Newcombe et al 2013 [69] | Periprosthetic bone stress vs. retained bone length | ITAP | 3D, CT, and Idealised Cylindrical | 1 | Instrumented prosthesis Axial and lateral forces and axial torque. | Anisotropic, inhomogeneous (5 models) | Ti-6Al-4V | 110 | 0.3 | Bonded | Bone axial and shear stress at implant-bone interface and bone outer surface |
| Stenlund et al 2016 [70] | Periprosthetic bone loading vs. bone geometry | OPRA | Idealised Cylindrical | 4 | Instrumented prosthesis in 5 individuals | Isotropic, two homogeneous regions (4 models) | Ti | 110 | 0.35 | Friction, μ=0.2 | Bone principal, axial and shear stress, and interface gap and displacements. |

KEY: ″ = ditto, as in same-group study listed above; CoCrMo = cobalt chromium molybdenum implant material alloy; CPTi = commercially pure titanium; CT = computed tomography imaging; E = Young's modulus, GPa; ISP Endo/Exo = commercial implant (ESKA Implants AG, Lübeck, Germany); ITAP = commercial implant (Stanmore Implants, Middlesex, UK); n = number of patients or geometries; N/S = not stated; OPRA = commercial implant (Integrum AB, Göteborg, Sweden); PEEK = poly-ether-ether-ketone polymer; $\nu$ = Poisson's ratio; Ti-6Al-4V = titanium implant material alloy; μ = coefficient of friction

ical risks associated with OI prostheses [98], especially given the high functional demands associated with the typical OI prosthesis user. One of the studies identified in this review did consider a fall load case [67], but the range of possible falling scenarios is wide, difficult to predict, and hard to reproduce in clinical studies. Researchers have attempted to reproduce falls in healthy individuals and infer corresponding loads on OI prostheses through multi-body simulation [107], and extensive analysis has been reported of an inadvertent fall which occurred during routine gait measurement [108].

#### 4.6.3. Bone–prosthesis-soft tissue modeling

To conclude this section, Yerneni et al. 2012 [65] performed the first study to include the OI implant–bone construct and the surrounding soft tissue structures, in order to assess the skin-abutment interface mechanics. They employed simplified geometry and loading conditions to generate maximum soft tissue shear, during sliding down a seating surface, during a seating transfer or rising from seated, and analyzed the generated radial stress in the skin around the implant–bone-skin junction. Their findings contribute early but clinically-relevant insights into preparation of the residual bone to enhance implant-skin adhesion, by encouraging stress dissipation, which is proposed to protect skin integrity. Their model was, necessarily, a simplified first representation of this region of the OI prosthesis construct. However, it lays an important foundation for further work on this primary barrier to bacterial infection, which remains a significant issue in individuals with OI prostheses [98,109], any may be of increasing importance as OI implantation by single-stage surgery becomes more common [110].

## 5. Areas of further interest, and recommendations

### 5.1. Un-investigated conditions, reconstructions and patient factors

To the authors' knowledge, there has been little or no research into several residual bone factors. At diaphyseal amputation levels, the residual bone will have an open-ended tubular shape immediately after surgery (Fig. 5A and C), with some degree of bevelling. Radiology provides extensive evidence of long term bone adaptation including generation of spurs due to HO (Fig. 5B and D), formation of aggressive bone edges, tumor growth, and bone bruises and fracture following trauma or adverse remodeling [111,112]. One of Portnoy's studies considered some aspects of distal tibia and fibula morphology [45], but published simulations of the causes and progression of adaptive bone remodeling were not found in this review, except where OI prostheses were used. Fundamentally, inspection of the methods reported in the cited studies indicates

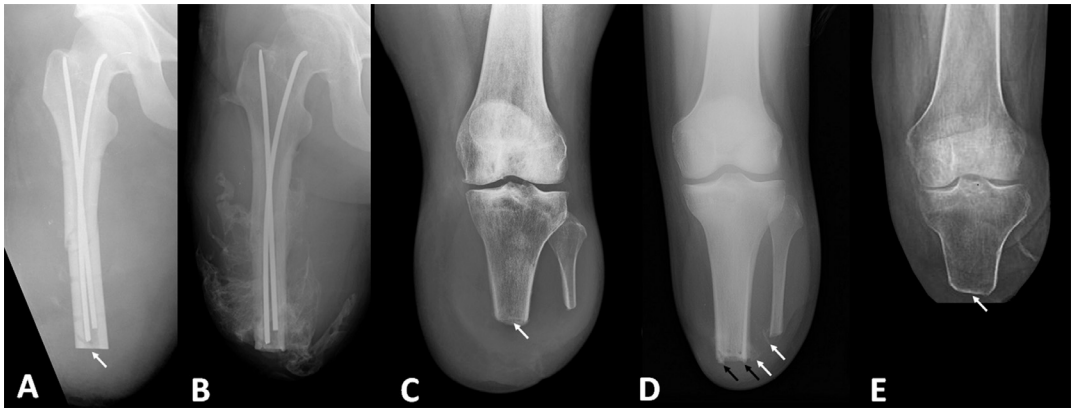


**Fig. 5.** Coronal residuum radiographs after A,B) above knee amputation for trauma, and C,D,E) below knee amputations. A,C) show an open medullary canal (white arrows); B,D) show formation of heterotopic ossification (white arrows) and aggressive bone edges (black arrows), and E) shows apparent cortex formation over osteotomy (white arrow).A, B) Reprinted from [172] with permission from Wolters Kluwer Health (licence 4054131375261), C) Sciencephoto.com (license 277,835/UNISOU09), D) Reprinted from [173] with permission from Wolters Kluwer Health (license 4026031374603), and E) Reprinted from [174], copyright © Nordic Orthopaedic Federation, with permission of Taylor & Francis Ltd, http://www.tandfonline.com on behalf of Nordic Orthopaedic Federation (license LA/IORT/P8879).

that solid, rigid bone models are most common. According to radiographic evidence the canal may close by establishing a neocortex (Fig. 5E). This may occur where there is exposed cancellous bone at the amputation level, but the bone morphology progression is unknown. Simple factors like this will have a substantial influence on predicted soft tissue strain.

Reports were limited to the most common transtibial and transfemoral amputation techniques. No analysis of bone-bridging transtibial amputations was found, although bridge fracture is understood to be a potential complication [113,114], and no models of knee disarticulation were found [115,116]. Considering the short- and long-term soft tissue adaptations known to occur, as suggested by Sanders in 2005 [21], no explicit consideration of muscle disuse atrophy and fatty infiltration has been made [117], which might provide evidence to support socket designs to maintain soft tissue health. Furthermore, future effort would be well directed towards mechanobiological simulations of the soft tissue healing process [118] including the influence of suturing, anisotropic soft tissue contraction, and the formation of granulation or scar tissue, also mentioned only by Portnoy et al. [45].

### 5.2. Loading conditions

Few of the cited studies have considered full dynamic loading conditions. Initial work on inverse dynamics from Jia et al. in 2004 [34] considering inertial effects represents the majority of citations for gait data in the present studies, in sagittal-plane 2D or full 3D. More recent 6-axis load cell gait analysis provides useful input force and moment data [119,120], and multi-individual analysis of residuum–socket moments has been conducted by Kobayashi et al. for transtibial sockets [121] and Highsmith et al. for transfemoral sockets [122], under different loading conditions.

As noted previously, for prediction of internal soft tissue strains, the full range of loading conditions should be applied, including residual strain from donning the socket and any liners. It was observed that no studies identified in this review mentioned simulation of a compression sock, commonly worn to help manage residuum volume, although Sanders, Cagle and co-workers have recently produced extensive experimental data which may facilitate this [123,124].

Adverse prosthetic limb loading should also be considered. Extensive work has been undertaken for OI patients whose limbs are fitted with load cells by Frossard and colleagues, including one report of fall data captured by chance [108]. Measuring or predicting such data in socket-suspended prosthetics is more difficult. Multi-body simulation work such as that by Schwarze et al. [125] will potentially enable investigation of more varied traumatic load cases which cannot be tested ethically. This requires a model of the dynamic coupling between the residuum and socket which accounts for axial pistoning and relative angular movements [126], which would not be captured in biomechanical modeling if traditional rigid body segment assumptions are made. Such a characterization of residual bone–prosthetic limb coupling could be achieved by FEA.

Recent work by Rigney, Simmons and Kark [127] has started to bring together multibody analysis of the lower limb with FEA of the prosthetic componentry, in order to provide more representative model boundary conditions for a running blade prosthesis case study. To date they have used a residual limb model with simplified cylindrical geometry in the cited report but they list a future goal of incorporating patient-specific residuum tissue geometry and mechanics.

### 5.3. Soft tissue modeling, and advances in imaging

A valuable target for further development in soft tissue modeling is the application of subject-specific tissue material parameters, recognizing that there will be inter-subject variations in many factors, including local damage and visceral fat content. This is especially common with diabetes and peripheral neuropathy [128] and disuse-atrophy after amputation [117], and can be characterized by fat-saturated MR imaging. Attempts may be made to characterize these properties using elastography [129–131] or by solving an inverse problem using FEA of comparative models built from unloaded and loaded MR images [89,132]. An extensive review of dynamic MR techniques for skeletal muscle is given by Prompers et al. [133].

One group of the identified studies used viscoelasticity and hyperelasticity at the continuum level to represent a range of material and structural nonlinearities of skeletal muscle. These effects arise from the tissue's hierarchical structure of fibers and extracellular matrix, the active–passive nature of the fibers, and the lymphatic and blood flows which may have compliance effects at the organ level. The cited reports have not yet considered skeletal muscle's anisotropy, perhaps owing to its primarily tensile loading during activity. Recent developments in continuum modeling most relevant to residual limb FEA have included hyperviscoelasticity and orthotropy under compressive loading [134], and in one of their papers Portnoy et al. implicitly accounted for the short

term change in muscle stiffness with activation [45] in their constitutive model parameters.

Further work may address the combined effects of viscoelastic-like behavior of tissues at the residual limb–socket construct level. This could incorporate changes in soft tissue compliance and shape due to tissue and organ level effects, such as elevated blood flow resulting from muscle activity, the effects of which can be measured in external residuum shape changes [135]. There may be scope to incorporate limb volume (unconstrained) [136], or muscle shape changes (constrained by a socket) due to the short term effects of activation. Furthermore, atrophy causes longer term changes in soft tissue shape [135] and mechanical properties. Modeling these effects may enable the loss of adequate socket fit to be predicted.

In all of the cited interface pressure studies, a single soft tissue bulk was assumed. Residuum inhomogeneity has been captured in most detail by Portnoy et al. [44,45,49], who separated the residuum into three soft tissue types, and assigned different constitutive model parameters to each (Table 3). Simple tissue geometry may be acceptable if prediction of tissue–prosthesis interface stresses are required, but if a study aims to characterize internal soft tissue conditions there may be value in modeling within-tissue inhomogeneity. This may be addressed both in material models and in identifying separate tissue structures, such as separate muscle compartments. One early study by Lee et al. [137] demonstrated the significant effects arising from defining separate muscle bodies in a transfemoral, 2D plane strain model, with material inhomogeneity and the possibility for intermuscular sliding. A more recent 2D model by Rohan et al. [138] considered the effects of compression stockings and muscular contraction upon the deformation of deep leg veins. In addition to these plane strain transverse section studies, 2D modeling has been used for simulations of an oblique section of transtibial residuums [43], and assuming axisymmetry of the residual femur-implant geometry [55]. These methods enable substantial savings in computational expense, as is required for real-time simulation, and high spatial resolution local to the model's region of interest. However, idealization of 3D geometry into a 2D representation is only appropriate in some cases, and there is limited scope to incorporate out-of-plane load variation. To consider macroscopic, organ-level structural effects, and the influence of load variation along and around the residuum, full 3D analysis is required. Image processing methods are reducing the computational intensiveness of such models, enabling expansion into 3D, but they may be difficult to validate. One promising approach could be the characterization of directional muscular inhomogeneity through fascicle visualization with diffusion tensor MRI [139]. This has been shown to give representative 3D muscle deformations upon activation in the gastrocnemius, by Fernandez [140]. This approach could enable more advanced muscle activation modeling than changing the material stiffness [45], and improve predictions of interfacial and internal tissue stress under dynamic conditions. Furthermore there is potential value of introducing within-tissue inhomogeneity in skin models, by consideration of the separate stratum corneum, viable epidermis and dermis layers. The range of potentially attributable material properties of these layers, and the effects of topographical features were demonstrated by Leyva-Mendivil et al. [141] and may be included explicitly (in the former case) or through multiscale modeling (in the latter), if the goal of modeling is to assess the potential for skin damage.

There is scope for further work on loading thresholds for tissue injury relating to the residual limb. Recent work by Loerakker et al. has presented more advanced strain/time thresholds for deep tissue damage incorporating load relief and reperfusion effects, demonstrated in animal DTI models under indenter loading [142–144]. This work and prior studies [77,78,80,81,90] have considered deep tissue injury, with a general focus on indentation and sustained support surface loading for people with conditions such as spinal cord injury. Linder-Ganz et al. also established that tissue stresses and strains are influenced by pathological anatomic changes, for their paraplegic seating study participants compared to a healthy group [145]. However, injury in residual limb soft tissues presents more commonly as superficial wounds and pressure ulcers [8–10], with markedly different loading and tissue characteristics. In order to evaluate soft tissue injury tolerance under these conditions, there would be value in further research with appropriate participant sub-populations, and under combined pressure and shear loading, as experienced at the prosthesis–skin interface. Both the resulting volumetric tissue strain and the host's ability to tolerate it will be affected by anatomic and tissue changes observed in diabetic disease and advanced muscle atrophy, as well as environmental factors such as temperature and humidity [13,76]. In association with prescribed mechanical deformations, a series of robust biomarkers could be utilized to monitor tissue health to inform strain thresholds. Measures could include local skin inflammation [146,147], ischemia [148] and lymphatic impairment [149].

### 5.4. Measurements for model validation

The most established interfacial force measurement systems are film pressure sensors [150,151] and discrete force transducers [152], which were reviewed in comparison to FEA predictions by Laing, et al. in 2011 [23]. Similar piezoelectric sensors have recently been proposed as a means for obtaining signals for active prosthetic limb control [153]. These produce normal tissue loading data only, and have limitations relating to precise pressure magnitude, gradient or contact area measurement, sensitivity to temperature and duration of pressure application, and the compliance of supporting surfaces [154]. There may also be limitations in applying these sensor films onto compound-curved surfaces due to in-plane stiffness and buckling or crinkling. Triaxial force transducers provide discreet point data and enable combined measurement of pressure and shear forces [152], but in the past had markedly higher stiffness than the residuum and required socket modification with windows for sensor application.

Use of flexible, isolated normal and shear force measurement sensors would be preferable. Recently, devices have been validated for this purpose [155,156] and first experiments conducted in an AKA socket [157]. Full-surface, high spatial resolution measurements are also desirable for FE model validation, which may be achieved using multiple sensors as described above, or textile sensors for pressure mapping [158]. Fiber Bragg Grating (FBG) sensors have also been proposed [159], and may have benefits in spatial resolution and capabilities in dynamic measurement, although the complexity and cost of peripheral equipment may preclude everyday use at present. Whilst the present review's findings demonstrate a shift in focus towards strain analysis of internal soft tissue structures, it is likely that surface stress predictions and measurements will continue to be valuable. Clinically, they offer a more practical and lower cost socket assessment capability than invasive volume imaging techniques. In numerical modeling, experimental measurement modalities with higher spatial resolution and sensitivity will enhance validation, which is important to maintain confidence in model predictions as their sophistication and complexity increases.

Finally, some established imaging techniques have been applied more recently to amputated lower limbs and may provide additional input data for model tuning or validation. Alongside upright MR scanning, fluoroscopy has been used to measure relative displacement between the residual bone and socket under quasi-static loading [160,161], simulated gait [162], and dynamic Roent-

gen stereophotogrammetric analysis has captured more strenuous activity [163].

## 6. Limitations

This review was conducted by engineers and health scientists only, so may demonstrate some interpretation bias. In an effort to prevent this, the main analysis was discussed with expert clinicians and other health scientists. The review also considered only publications in the English language literature, except for two cases where authors assisted with translation or interpretation.

## 7. Conclusion

Numerical modeling of the amputated limb has received less attention than many other musculoskeletal conditions, partially due to the smaller incidence of lower limb amputation than, for example, total joint replacement. However, the potential quality of life benefits of improving the comfort of the residual limb–prosthetic limb interface are substantial, for the life of the prosthetic limb user. From a purely mechanical perspective, however, the modeling complexity is high, featuring multi-body structures connected by contact pairs, highly nonlinear material models, and dynamic, variable loading conditions. Complicating matters further, inter- and intra-individual loading and anatomic variability are large, and influenced by surgical variability and prosthetic prescription. Extensive progress has been made in the interpretation of model predictions, considering thresholds for tissue injury and adverse adaptation. Other researchers have also attempted to include factors such as comfort and pain threshold, which are highly subjective and difficult to evaluate.

There is value in working towards highly accurate and detailed user-specific biomechanical models, but a key practical value in limb–prosthesis FE models is in contributing to evidence-based prosthetic limb fitting, and such a model's requirements would be rather different. Parametric models may enable comparative analysis of different prosthetic limb options, and the identification of potential risk factors, and worst cases for pre-clinical analysis of new technologies. Despite the described progress towards a clinically-translatable FE model automated user-specific socket design [38], these methods are still not in clinical use. Several considerations should be made for overcoming the barriers to clinical translation, which are common with all clinical decision-support tools. Experience of introducing IT systems in 1990s showed that the success of technology adoption is linked to the implementation management process and the receptiveness of clinicians [164]. This receptiveness, as well as the safety of the technology's use, are enhanced when technology is developed with end-user involvement [165]. Considering FEA in prosthetic limb fitting, collaboration with clinicians will enable the development of appropriate measurement methods to obtain model input data. Furthermore, appropriate design architecture may be developed, such that expert engineering input is not required [47]. Technically, simulations will require an optimal balance of computational expense and accuracy so that there is no assumption that high performance computing hardware or expensive commercial FEA software licences are procured by each clinic. As important, the use of a new clinical technology must not increase consultation time or cost, or impede the application of the users' skill. This is essential in prosthetics and orthotics, where the clinical consultation is so personalized, and limb assessment through processes such as palpation are at the center of the clinician's application of their skill and experience.

## Conflict of interest

There is no potential conflict of interest. The authors did not receive and will not receive any direct or indirect benefits from third parties for the performance of this study.

## Acknowledgments

Funding: The authors would like to thank the following for their financial support:

ASD: the Royal Academy of Engineering, UK, (ref RF/130),

JWS: the University of Southampton's EPSRC Doctoral Training Program (DTP, block grant), and

PRW: the EPSRC–NIHR "Medical Device and Vulnerable Skin Network" (ref EP/M000303/1).

Supporting data is openly available from the University of Southampton repository at http://dx.doi.org/10.5258/SOTON/402198.

## Appendix

Summary of Hyperelasticity in ABAQUS (Simulia, RI, USA) and Portnoy et al's Notation

In linear elasticity and tensor notation, Hooke's law in 3D is given by:

$$\boldsymbol{\sigma} = \lambda tr(\boldsymbol{\varepsilon}) I + 2G\boldsymbol{\varepsilon} \tag{5}$$

where $\boldsymbol{\sigma}$ is the infinitesimal stress tensor:

$$\boldsymbol{\sigma} = \begin{bmatrix} \sigma_{11} & \sigma_{12} & \sigma_{13} \\ \sigma_{21} & \sigma_{22} & \sigma_{23} \\ \sigma_{31} & \sigma_{32} & \sigma_{33} \end{bmatrix} \tag{6}$$

and $\boldsymbol{\varepsilon}$ is the infinitesimal strain tensor:

$$\boldsymbol{\varepsilon} = \begin{bmatrix} \varepsilon_{11} & \varepsilon_{12} & \varepsilon_{13} \\ \varepsilon_{21} & \varepsilon_{22} & \varepsilon_{23} \\ \varepsilon_{31} & \varepsilon_{32} & \varepsilon_{33} \end{bmatrix} \tag{7}$$

and where $I$ is the second order identity tensor. $\lambda$ and $G$ are the two Lamé coefficients, which are given in terms of two material constants, the Young's modulus $E$ and the Poisson's ratio $\nu$:

$$\lambda = \frac{E\nu}{(1+\nu)(1-2\nu)} \quad \text{and} \quad G = \frac{E}{2(1+\nu)} \tag{8}$$

$G$ is the shear modulus, the elasticity modulus for shear or torsion.

If the linear elastic material model is extended simply, the strain energy density ($W$), a scalar, is given by the St. Venant–Kirchhoff model:

$$W = \frac{1}{2}\lambda[tr(\boldsymbol{\varepsilon})]^2 + Gtr(\boldsymbol{\varepsilon})^2 \tag{9}$$

Hyperelasticity has been defined in the cited studies by constitutive models, which relate a strain energy density function to stretch (strain plus 1) as a function of one or more invariants of a deformation tensor [166]. The left and right Cauchy-Green deformation tensors ($\boldsymbol{b}$ and $\boldsymbol{C}$) are commonly used:

$$\boldsymbol{b} = \boldsymbol{F} \cdot \boldsymbol{F}^T, \quad \text{and} \quad \boldsymbol{C} = \boldsymbol{F}^T \cdot \boldsymbol{F} \tag{10}$$

where $\boldsymbol{F}$ is the deformation gradient $\partial \boldsymbol{x}/\partial \boldsymbol{X}$, and can be defined in terms of the principal stretch ratios $\lambda_i$:

$$\boldsymbol{F} = \begin{bmatrix} \lambda_1 & 0 & 0 \\ 0 & \lambda_2 & 0 \\ 0 & 0 & \lambda_3 \end{bmatrix} \tag{11}$$

From Rivlin [166], for an isotropic incompressible material where the total volume ratio $J = det(\boldsymbol{F}) = \lambda_1\lambda_2\lambda_3 = 1$, the deformation tensor invariants are:

$$I_1 = \lambda_1^2 + \lambda_2^2 + \lambda_3^2, \quad \text{and}$$

$$I_2 = \lambda_2^2\lambda_3^2 + \lambda_3^2\lambda_1^2 + \lambda_1^2\lambda_2^2 \equiv \lambda_1^{-2} + \lambda_2^{-2} + \lambda_3^{-2} \tag{12}$$

A Neo-Hookean model was developed for rubber materials by Treloar [167] with the assumption of incompressibility. This allows initially linear stress–strain behavior, and non-linear behavior after a defined threshold level. Its strain energy density function considers the first deformation tensor invariant $I_1$ and the shear modulus only:

$$W_{NH} = \frac{G}{2}(I_1 - 3) \tag{13}$$

Treloar demonstrated its validity for compression but showed shortcomings in tension and shear [168]. This was followed by what is commonly referred to as the Mooney-Rivlin model [166,169], which was reported to agree with experimental data for soft rubber at strains between 50% compression and 400% extension:

$$W_{MR} = C_{10}(I_1 - 3) + C_{01}(I_2 - 3) \tag{14}$$

and

$$G = 2(C_{10} + C_{01}) \tag{15}$$

Compressibility can be included by removing the restriction that the volume ratio $J=1$, and constructing the SED from separate deviatoric $W_d$ and volumetric $W_v$ terms. Deviatoric strain invariants are used, which are functions of the deviatoric stretches ($\bar{\lambda}_i$):

$$\bar{I}_1 = \bar{\lambda}_1^2 + \bar{\lambda}_2^2 + \bar{\lambda}_3^2 \quad \text{and} \quad \bar{I}_2 = \bar{\lambda}_1^{-2} + \bar{\lambda}_2^{-2} + \bar{\lambda}_3^{-2} \tag{16}$$

The deviatoric stretches are related to the principal stretches as a function of the total volume ratio:

$$\bar{\lambda}_i = J^{-1/3}\lambda_i \tag{17}$$

In the case of incompressible materials ($J=1$), these are equivalent.

For example, compressibility can be added as an extension to the Neo-Hookean model:

$$W = W_d + W_v = C_{10}\left(\bar{I}_1 - 3\right) + \frac{1}{D_1}(J-1)^2 \tag{18}$$

$C_{10}$ and $D_1$ are constitutive model parameters, with $C_{10}$ still equal to half the shear modulus, and $D_1$ related to the bulk modulus $K$, where:

$$D_1 = \frac{2}{K} \tag{19}$$

$$K = \frac{E}{3(1-2\nu)} = \frac{2G(1+\nu)}{3(1-2\nu)} \tag{20}$$

The strain energy density function was proposed to be an infinite expansion of the two deformation tensor invariants $I_1$ and $I_2$ by Mooney [169] and Rivlin [166], given in general form by Ogden [170]:

$$W = \sum_{i,j=0}^{\infty} C_{ij}(I_1 - 3)^i(I_2 - 3)^j \qquad (C_{00} = 0) \tag{21}$$

and is alternatively given in generalized polynomial form, with polynomial order $m$:

$$W = \sum_{i+j=1}^{m} C_{ij}(I_1 - 3)^i(I_2 - 3)^j \tag{22}$$

Finally, the generalized polynomial form can be modified to include compressibility effects:

$$W = \sum_{i+j=1}^{m} C_{ij}\left(\bar{I}_1 - 3\right)^i\left(\bar{I}_2 - 3\right)^j + \sum_{i=1}^{m}\frac{1}{D_1}(J-1)^{2i} \tag{23}$$

with general constitutive model parameters $C_{ij}$ and $D_1$.

The Neo-Hookean and Mooney Rivlin models are 1st order formulations, used to model scar, fat muscle, and combined soft tissues by the studies identified in the present review (Table 3). The extended Mooney model is a 2nd order formulation, used to represent skin:

$$W = C_{10}(I_1 - 3) + C_{11}(I_1 - 3)(I_2 - 3) \tag{24}$$

Finally, the James-Green–Simpson model is a 3rd order formulation, which has been used to represent the combined structure of soft tissue layers together [29,33]:

$$W = C_{10}(I_1 - 3) + C_{01}(I_2 - 3) + C_{11}(I_1 - 3)(I_2 - 3) + C_{20}(I_1 - 3)^2 + C_{30}(I_1 - 3)^3 \tag{25}$$

and can be simplified with an axisymmetric assumption (where there is zero angular displacement, so zero circumferential stretch, and therefore $I_1 = I_2$) such that:

$$W = 2C_{10}(I_1 - 3) + 2C_{20}(I_1 - 3)^2 + C_{30}(I_1 - 3)^3 \tag{26}$$

which is very similar to the reduced third order polynomial Yeoh model [171].

The derivative of the strain energy function with respect to a particular strain component $\varepsilon_{ij}$ gives the corresponding stress component $\sigma_{ij}$:

$$\sigma_{ij} = \frac{\delta W}{\delta \varepsilon_{ij}} \tag{27}$$

and these SED functions are employed by performing an empirical fit of a proposed material model to experimental stress–strain experimental data, by selecting appropriate terms and constitutive model parameter values for $C_{ij}$ and $D_1$.

A typical modeling formulation [44] employing FE package ABAQUS is to calculate the finite strain 'Green-Lagrange strain tensor'

$$\boldsymbol{E} = \frac{1}{2}(\boldsymbol{C} - \boldsymbol{I}) \tag{28}$$

using applied bone displacement boundary conditions, from which the 'second Piola-Kirchhoff stress tensor' ($\boldsymbol{S}$) is calculated:

$$\boldsymbol{S} = \frac{\partial W}{\partial E} \tag{29}$$

and finally the Cauchy (true) stress tensor ($\boldsymbol{\sigma}$) can be derived:

$$\boldsymbol{\sigma} = J^{-1}\boldsymbol{F}\cdot\boldsymbol{S}\cdot\boldsymbol{F}^T \tag{30}$$

These stresses are then plotted as in conventional linear elastic FEA, used as described in the main text to calculate tissue damage risk predictions in comparison to threshold damage levels, and equivalent stress magnitude (often referred to in FEA packages as 'von Mises' stress).

## References


[1] ISPO Triennium Report 2010 - 2013. 2013, International Society for Prosthetics and Orthotics: Brussels.

[2] Rommers GM, Vos LDW, Klein L, Groothoff JW, Eisma WH. A study of technical changes to lower limb prostheses after initial fitting. Prosthet Orthot Int 2000;24:28–38.

[3] Häggström E, Hansson E, Hagberg K. Comparison of prosthetic costs and service between osseointegrated and conventional suspended transfemoral prostheses. Prosthet Orthot Int 2013;37:152–60.

[4] Lilja M, Oberg T. Proper time for definitive transtibial prosthetic fitting. J Prosthet Orthot 1997;9(2):90–5.

[5] Lilja M, Hoffmann P, Oberg T. Morphological changes during early trans-tibial prosthetic fitting. Prosthet Orthot Int 1998;22:115–22.

[6] Zachariah SG, Saxena R, Fergason JR, Sanders JE. Shape and volume change in the transtibial residuum over the short term: preliminary investigation of six subjects. J Rehabil Res Dev 2004;41(5):683–94.

[7] Gailey R, Allen K, Castles J, Kucharik J, Roeder M. Review of secondary physical conditions associated with lower-limb amputation and long-term prosthesis use. J Rehab Res Dev 2008;45(1):15–30.

[8] Lyon CC, Kulkarni J, Zimerson E, Van Ross E, Beck MH. Skin disorders in amputees. J Am Acad Dermatol 2000;42:501–7.
[9] Levy SW. Skin problems of the leg amputee. Prosthet Orthot Int 1980;4:37–44.
[10] Salawu A, Middleton C, Gilbertson A, Kodavali K, Neumann V. Stump ulcers and continued prosthetic limb use. Prosthet Orthot Int 2006;30(3):279–85.
[11] Ibbontson SH, Simpson NB, Fyfe NC, Lawrence CM. Follicular keratoses at amputation sites. Br J Dermatol 1994;130(6):770–2.
[12] Bouten CV, Oomens CW, Baaijens FP, Bader DL. The etiology of pressure ulcers: skin deep or muscle bound? Arch Phys Med Rehabil 2003;84:616–19.
[13] Meulenbelt HEJ, Geertzen JHB, Dijkstra PU, Jonkman MF. Skin problems in lower limb amputees: an overview by case reports. J Eur Acad Dermatol Venereol 2007;21:147–55.
[14] Baars ECT, Geertzen JHB. A patient with donning-related stump wounds: a case report. Prosthet Orthot Int 2008;32(2):219–22.
[15] Gefen A, van Nierop B, Bader DL, Oomens CW. Strain-time cell-death threshold for skeletal muscle in a tissue-engineered model system for deep tissue injury. J Biomech 2008;41:2003–12.
[16] Torres-Moreno R, Jones D, Solomonides SE, Mackie H. Magnetic resonance imaging of residual soft tissues for computer-aided technology applications in prosthetics - a case study. J Prosthet Orthot 1999;11(1):6–11.
[17] Moher D, Liberati A, Tetzlaff J, Altman DG. Preferred reporting items for systematic reviews and meta-analyses: the PRISMA statement. PLoS Med 2009;6(7):e1000097.
[18] Silver-Thorn MB, Steege JW, Childress DS. A review of prosthetic interface stress investigations. J Rehab Res Dev 1996;33(3):253–66.
[19] Zachariah SG, Sanders JE. Interface mechanics in lower-limb external prosthetics: a review of finite element methods. IEEE Trans Rehab Eng 1996;4(4):288–302.
[20] Zhang M, Mak AFT, Roberts VC. Finite element modeling of a residual lower-limb in a prosthetic socket: a survey of the development in the first decade. Med Eng Phys 1998;20:360–73.
[21] Sanders JE. Stump-socket interface conditions. Pressure ulcer research, current and future perspectives. Bader DL, Bouten C, Colin D, Oomens C, editors. Springer; 2005.
[22] Collins DM, Karmarkar A, Relich R, Pasquina PF, Cooper RA. Review of research on prosthetic devices for lower extremity amputation. Crit Rev Biomed Eng 2006;34(5):379–438.
[23] Laing S, Lee PVS, Goh JCH. Engineering a trans-tibial prosthetic socket for the lower limb amputee. Ann Acad Med Singap 2011;40:252–9.
[24] Pirouzi G, Abu Osman NA, Eshraghi A, Ali S, Gholizadeh H, Wan Abas WAB. Review of the socket design and interface pressure measurement for transtibial prosthesis. World Sci J 2014;849073.
[25] Ginestra PS, Ceretti E, Fiorentino A. Potential of modeling and simulations of bioengineered devices: endoprostheses, prostheses and orthoses. Proc IMechE Part H: J Eng Med 2016;230(7):607–38.
[26] Zhang M, Roberts C. Comparison of computational analysis with clinical measurement of stresses on below-knee residual limb in a prosthetic socket. Med Eng Phys 2000;22(9):607–12.
[27] Zachariah SG, Sanders JE. Finite element estimates of interface stress in the transtibial prosthesis using gap elements are different from those using automated contact. J Biomech 2000;33:895–9.
[28] Amali R, et al. A novel approach for assessing interfacial pressure between the prosthetic socket and the residual limb for below knee amputees using artificial neural networks.. In: Ijcnn'01: international joint conference on neural networks, Vols 1-4; 2001. p. 2689–93. Proceedings.
[29] Tonuk E, Silver-Thorn MB. Nonlinear elastic material property estimation of lower extremity residual limb tissues. IEEE Trans Neural Syst Rehab Eng 2003;11(1):43–53.
[30] Wu C-L, Chang C-H, Hsu A-T, Lin C-C, Chen S-I, Chang G-L. A proposal for the pre-evaluation protocol of below-knee socket design integration pain tolerance with finite element analysis. J Chin Inst Eng 2003;26(6):853–60.
[31] Lin C-C, Chang C-H, Wu C-L, Chung K-C, Liao I-C. Effects of liner stiffness for trans-tibial prosthesis a finite element contact model. Med Eng Phys 2004;26:1–9.
[32] Lee WCC, Zhang M, Jia X, Cheung JTM. Finite element modeling of the contact interface between trans-tibial residual limb and prosthetic socket. Med Eng Phys 2004;26(8):655–62.
[33] Tonuk E, Silver-Thorn MB. Nonlinear viscoelastic material property estimation of lower extremity residual limb tissues. J Biomech Eng 2004;126:289–300.
[34] Jia X, Zhang M, Lee WCC. Load transfer mechanics between trans-tibial prosthetic socket and residual limb - dynamic effects. J Biomech 2004;37:1371–7.
[35] Lee WCC, Zhang M, Boone DA, Contoyannis B. Finite-element analysis to determine the effect of monolimb flexibility on structural strength and interaction between residual limb and prosthetic socket. J Rehab Res Dev 2004;41(6A):775–86.
[36] Jia X, Zhang M, Li X, Lee WCC. A quasi-dynamic nonlinear finite element model to investigate prosthetic interface stresses during walking for trans-tibial amputees. Clin Biomech 2005;20:630–5.
[37] Lee WCC, Zhang M, Mak AF. Regional differences in pain threshold and tolerance of the transtibial residual limb: including the effects of age and interface material. Arch Phys Med Rehab 2005;86(4):641–9.
[38] Goh JCH, et al. Development of an integrated CAD-FEA process for below-knee prosthetic sockets. Clin Biomech 2005;20(6):623–9.
[39] Faustini MC, Neptune RR, Crawford RH. The quasi-static response of compliant prosthetic sockets for transtibial amputees using finite element methods. Med Eng Phys 2006;28:114–21.
[40] Peery JT, Klute GK, Blevins JJ, Ledoux WR. A three-dimensional finite element model of the transibial residual limb and prosthetic socket to predict skin temperatures. IEEE Trans Neural Syst Rehab Eng 2006;14(3):336–43.
[41] Liu Z, Fan Y, Qian Y, Zhang M. Biomechanical research of the endoskeletal trans-tibial monolimb. In: 2007 IEEE/ICME international conference on complex medical engineering; 2007. p. 1295–9.
[42] Lee WCC, Zhang M. Using computational simulation to aid in the prediction of socket fit: a preliminary study. Med Eng Phys 2007;29(8):923–9.
[43] Portnoy S, Yarnitzky G, Yizhar Z, Kristal A, Oppenheim U, Siev-Ner I, et al. Real-time patient specific finite element analysis of internal stresses in the soft tissues of a residual limb: a new tool for prosthetic fitting. Ann Biomed Eng 2007;35(1):120–35.
[44] Portnoy S, Yizhar Z, Shabshin N, Itzchak Y, Kristal A, Dotan-Marom Y, et al. Internal mechanical conditions in the soft tissues of a residual limb of a trans-tibial amputee. J Biomech 2008;41:1897–909.
[45] Portnoy S, et al. Surgical and morphological factors that affect internal mechanical loads in soft tissues of the transtibial residuum. Ann Biomed Eng 2009;37(12):2583–605.
[46] Portnoy S, et al. Patient-specific analyses of deep tissue loads post transtibial amputation in residual limbs of multiple prosthetic users. J Biomech 2009;42(16):2686–93.
[47] Portnoy S, van Haare J, Geers RPJ, Kristal A, Siev-Ner I, Seelen HAM, et al. Real-time subject-specific analyses of dynamic internal tissue loads in the residual limb of transtibial amputees. Med Eng Phys 2010;32:312–23.
[48] Colombo G, Filippi S, Rizzi C, Rotini F. A new design paradigm for the development of custom-fit soft sockets for lower limb prostheses. Comput Ind 2010;61:513–23.
[49] Portnoy S, et al. Effects of sitting postures on risks for deep tissue injury in the residuum of a transtibial prosthetic-user: a biomechanical case study. Comput Methods Biomech Biomed Eng 2011;14(11):1009–19.
[50] Sengeh DM, Moerman KM, Petron A, Herr H. Multi-material 3-D viscoelastic model of a transtibial residuum from in-vivo indentation and MRI data. J Mech Behav Biomed Mater 2016;59:379–92.
[51] Lacroix D, Ramirez Patino JF. Finite element analysis of donning procedure of a prosthetic transfemoral socket. Ann Biomed Eng 2011;39(12):2972–83.
[52] Ramírez JF, Vélez JA. Incidence of the boundary condition between bone and soft tissue in a finite element model of a transfemoral amputee. Prosthet Orthot Int 2012;36:405–14.
[53] Zhang L, et al. Finite element analysis of the contact interface between trans-femoral stump and prosthetic socket. In: 2013 35th annual international conference of the IEEE engineering in medicine and biology society (Embc); 2013. p. 1270–3.
[54] Velez Zea JA, Bustamante Goez LM, Villarraga Ossa JA. Relation between residual limb length and stress distribution over stump for transfemoral amputees. Revista EIA (Spanish) 2015;12(23):107–15.
[55] Xu W, Crocombe AD, Hughes SC. Finite element analysis of bone stress and strain around a distal osseointegrated implant for prosthetic limb attachment. Proc IMechE Part H: J Eng Med 2000;214:595–602.
[56] Zheng L, Luo JM, Yang BC, Chen JY, Zhang XD. 3D finite element analysis of bone stress around distally osteointegrated implant for artificial limb attachment. Key Eng Mater 2005;288-289:653–6.
[57] Xu W, Xu DH, Crocombe AD. Three-dimensional finite element stress and strain analysis of a transfemoral osseointegration implant. Proc Inst Mech Eng Part H-J Eng Med 2006;220(H6):661–70.
[58] Lee W, Frossard L, Cairns N, Branemark R, Evans J, Adam C, et al. Finite element modeling to aid in refining the rehabilitation of amputees using osseointegrated prostheses. In: Duffy VG, editor. Digital human modeling; 2007. p. 655–8.
[59] Lee WCC, Doocey JM, Branemark R, Adam CJ, Evans JH, Pearcy MJ, et al. FE stress analysis of the interface between the bone and an osseointegrated implant for amputees - Implications to refine the rehabilitation program. Clin Biomech 2008;23(10):1243–50.
[60] Xu W, Robinson K. X-ray image review of the bone remodeling around an osseointegrated trans-femoral implant and a finite element simulation case study. Ann Biomed Eng 2008;36(3):435–43.
[61] Helgason B, et al. Risk of failure during gait for direct skeletal attachment of a femoral prosthesis: a finite element study. Med Eng Phys 2009;31(5):595–600.
[62] Isaacson BM, et al. Developing a quantitative measurement system for assessing heterotopic ossification and monitoring the bioelectric metrics from electrically induced osseointegration in the residual limb of service members. Ann Biomed Eng 2010;38(9):2968–78.
[63] Tomaszewski PK, et al. A comparative finite-element analysis of bone failure and load transfer of osseointegrated prostheses fixations. Ann Biomed Eng 2010;38(7):2418–27.
[64] Isaacson BM, Stinstra JG, Bloebaum RD, Pasquina PF, Macleod RS. Establishing multiscale models for simulating whole limb estimates of electric fields for osseointegrated implants. IEEE Trans Biomed Eng 2011;58(10):2991–4.
[65] Yerneni S, Dhaher Y, Kuiken TA. A computational model for stress reduction at the skin-implant interface of osseointegrated prostheses. J Biomed Mater Res Part A 2012;100A(4):911–17.

[66] Tomaszewski PK, et al. Simulated bone remodeling around two types of osseointegrated implants for direct fixation of upper-leg prostheses. J Mech Behav Biomed Mater 2012;15:167–75.
[67] Tomaszewski PM, et al. Numerical analysis of an osseointegrated prosthesis fixation with reduced bone failure risk and periprosthetic bone loss. J Biomech 2012;45(11):1875–80.
[68] Tomaszewski PK, et al. Experimental assessment of a new direct fixation implant for artificial limbs. J Mech Behav Biomed Mater 2013;21:77–85.
[69] Newcombe L, et al. Effect of amputation level on the stress transferred to the femur by an artificial limb directly attached to the bone. Med Eng Phys 2013;35(12):1744–53.
[70] Stenlund P, Trobos M, Lausmaa J, Brånemark R, Thomsen P, Palmquist A. Effect of load on the bone around bone-anchored amputation prostheses. J. Orthop. Res. 2016. doi:10.1002/jor.23352.
[71] Krouskop TA, Muilenberg AL, Doughtery DR, Winningham DJ. Computer-aided design of a prosthetic socket for an above-knee amputee. J Rehab Res Dev 1987;24(2):31–8.
[72] Sanders JE, Greve JM, Mitchell SB, Zachariah SG. Material properties of commonly-used interface materials and their static coefficients of friction with skin and socks. J Rehab Res Dev 1998;35(2):161–76.
[73] Zhang M, Mak AFT. In vivo properties of human skin. Prosthet Orthot Int 1999;23:135–41.
[74] Derler S, Gerhardt L-C. Tribology of skin: review and analysis of experimental results for the friction coefficient of human skin. Tribol Lett 2012;45:1–27.
[75] Ramirez JF, Pavon JJ, Toro A. Experimental assessment of friction coefficient between polypropylene and human skin using instrumented sclerometer. Proc IMechE Part J: J Eng Tribol 2015;229(3):259–65.
[76] Gefen A. How do microclimate factors affect the risk for superficial pressure ulcers: a mathematical modeling study. J Tissue Viability 2011;20(3):81–8.
[77] Oomens CWJ, Loerakker S, Bader DL. The importance of internal strain as opposed to interface pressure in the prevention of pressure related deep tissue injury. J Tissue Viability 2010;19:35–42.
[78] Ceelen KK, Stekelenburg A, Loerakker S, Strijkers GJ, Bader DL, Nicolay K, et al. Compression-induced damage and internal tissue strains are related. J Biomech 2008;41:3399–404.
[79] Sanders JE, Daly CH. Normal and shear stresses on a residual limb in a prosthetic socket during ambulation - comparison of finite-element results with experimental measurements. J Rehab Res Dev 1993;30(2):191–204.
[80] Linder-Ganz E, Engelberg S, Scheinowitz M, Gefen A. Pressure-time cell death threshold for albino rat skeletal muscles as related to pressure sore biomechanics. J Biomech 2006;39:2725–32.
[81] Gefen A, Gefen N, Linder-Ganz E, Marguiles SS. In vivo muscle stiffening under bone compression promotes deep pressure sores. J Biomech Eng 2005;127:512–24.
[82] Hendricks FM, Brokken D, van Eemeren JTWM, Oomens CWJ, Baaijens FPT, Horsten JBAM. A numerical-experimental method to characterize the non–linear mechanical behaviour of human skin. Skin Res Technol 2003;9:274–83.
[83] Zhang M, Lord M, Turner-Smith AR, Roberts VC. Development of a nonlinear finite-element modeling of the below-knee prosthetic socket interface. Med Eng Phys 1995;17(8):559–66.
[84] Peery JT, Ledoux WR, Klute GK. Residual-limb skin temperature in transtibial sockets. J Rehab Res Dev 2005;42(2):147–54.
[85] Clark M, Romanelli M, Reger SI, Ranganathan VK, Black J, Dealey C. Microclimate in context. International review: pressure ulcer prevention: pressure, shear, friction and microclimate in context. MacGregor L, editor. Wounds International; 2010.
[86] See-Sia W, Wipke-Tevis DD, Williams DA. Elevated sacral skin temperature (Ts): a risk factor for pressure ulcer development in hospitalized neurologically impaired Thai patients. Appl Nurs Res 2005;18(1):29–35.
[87] Atherton DJ. A review of the pathophysiology, prevention and treatment of irritant diaper dermatitis. Curr Med Res Opin 2004;20(5):645–9.
[88] Gerhardt L-C, Strassle V, Lenz A, Spencer ND, Derler S. Influence of epidermal hydration on the friction of human skin against textiles. J R Soc Interface 2008;5:1317–28.
[89] Avril S, Bouten L, Dubuis L, Drapier S, Pouget J. Mixed Experimental and Numerical Approach for Characterizing the Biomechanical Response of the Human Leg Under Elastic Compression. ASME. J Biomech Eng 2010;132(3):031006-031006-8. doi:10.1115/1.4000967.
[90] Linder-Ganz E, Shabshin N, Itzchak Y, Gefen A. Assessment of mechanical conditions in sub-dermal tissues during sitting: a combined experimental-MRI and finite element approach. J Biomech 2007;40:1443–54.
[91] Palevski A, Glaich I, Portnoy S, Linder-Ganz E, Gefen A. Stress relaxation of porcine gluteus muscle subjected to sudden transverse deformation as related to pressure sore modeling. J Biomech Eng 2006;128:782–7.
[92] Reynolds DP, Lord M. Interface load analysis for computer-aided design of below-knee prosthetic sockets. Med Biol Eng Comput 1992;30:419–26.
[93] Frillici FS, Rissone P, Rizzi C, Rotini F. The role of simulation tools to innovate the prosthesis socket design process. Innovative production machines and systems. Pham DT, Eldukhri EE, Soroka AJ, editors. Cardiff University, UK: MEC; 2008.
[94] Colombo G, Facocetti G, Rizzi C. Automatic below-knee prosthesis socket design: a preliminary approach. In: 7th international digital human modeling conference: applications in health, safety, ergonomics and risk management, Toronto, Canada. Springer; 2016.
[95] Omasta M, Paloušek D, Návrat T, Rosický J. Finite element analysis for the evaluation of the structural behaviour, of a prosthesis for trans-tibial amputees. Med Eng Phys 2012;34:38–45.
[96] Sengeh DM, Herr H. A variable-impedance prosthetic socket for a transtibial amputee designed from magnetic resonance imaging data. J Prosthet Orthot 2013;25:129–37.
[97] Brånemark R, Brånemark P-I, Rydevik B, Myers R. Osseointegration in skeletal reconstruction and rehabilitation: a review. J Rehab Res Dev 2001;38(2):175–81.
[98] Sullivan J, Uden M, Robinson KP, Sooriakumaran S. Rehabilitation of the trans-femoral amputee with an osseointegrated prosthesis: the United Kingdom experience. Prosthet Orthot Int 2003;27:114–20.
[99] Aschoff HH, Kennon RE, Keggi JM, Rubin LE. Transcutaneous, distal femoral, intramedullary attachment for above-the-knee prostheses: an endo-exo device. J Bone Joint Surg [Am] 2010;92(Suppl 2):180–6.
[100] Hagberg K, Brånemark R, Gunterberg B, Rydevik B. Osseointegrated trans-femoral amputation prostheses: prospective results of general and condition-specific quality of life in 18 patients at 2 year follow-up. Prosthet Orthot Int 2008;32:29–41.
[101] Branemark R, Berlin O, Hagberg K, Bergh P, Gunterberg B, Rydevik B. A novel osseointegrated percutaneous prosthetic system for the treatment of patients with transfemoral amputation. A prospective study of 51 patients. Bone Joint J 2014;96-B:106–13.
[102] Krouskop TA, Trono R, Adamski AJ. Effects of pylon shape on bone-pylon interface performance in direct skeletal attachment. J Biomed Mater Res 1976;10(3):345–69.
[103] Thompson ML, Backman D, Branemark R, Mechefske CK. Evaluating the bending response of two osseointegrated transfemoral implant systems using 3D digital image correlation. ASME. J Biomech Eng. 2011;133(5):051006-051006-9. doi:10.1115/1.4003871.
[104] Chanda S, Dickinson AS, Gupta S, Browne M. Full-field in vitro measurements and in silico predictions of strain shielding in the implanted femur after total hip arthroplasty. Proc IMechE Part H: J Eng Med 2015;229:549–59.
[105] Potter BK, Scoville CR. Amputation is not isolated: an overview of the US army amputee patient care program and associated amputee injuries. J Am Acad Orthop Surg 2006;14:S188–90.
[106] Frossard LA, Häggström E, Hagberg K, Brånemark R. Load applied on a bone-anchored transfemoral prosthesis: characterisation of a prosthesis - a pilot study. J Rehab Res Dev 2013;50(5):619–34.
[107] Welke B, Schwarze M, Hurschler C, Calliess T, Seehaus F. Multibody simulation of various falling scenarios for determining resulting loads at the prosthesis interface of transfemoral amputees with osseointegrated fixation. J Orth Res 2013;31:1123–9.
[108] Frossard LA, Tranberg R, Haggstrom E, Pearcy M, Brånemark R. Load on osseointegrated fixation of a transfemoral amputee during a fall: loading, descent, impact and recovery analysis. Prosthet Orthot Int 2010;34:85–97.
[109] Tillander J, Hagberg K, Hagberg L, Branemark R. Osseointegrated titanium implants for limb prostheses attachments. Infectious complications. Clin Orth Rel Res 2010;468:2781–8.
[110] Khemka A, Frossard L, Lord S, Bosley B, Al Muderis M. Osseointegrated prosthetic limb for amputees: single stage surgery. In: 6th international conference on advances in orthopaedic osseointegration, Las Vegas, Nevada; 2015.
[111] Baumgartner R, Langlotz M. Amputee stump radiology. Prosthet Orthot Int 1980;4:97–100.
[112] Henrot P, Stines J, Walter F, Martinet N, Paysant J, Blum A. Imaging of the painful lower limb stump. Radiographics 2000;20:S219–35.
[113] Loon HE. Below-knee amputation surgery. Artif Limbs 1962;6(2):86–99.
[114] Pinto MAGS, Harris WW. Fibular segment bone bridging in trans-tibial amputation. Prosthet Orthot Int 2004;28:220–4.
[115] Murakami T, Murray K. Outcomes of knee disarticulation and the influence of surgical techniques in dysvascular patients: a systematic review. Prosthet Orthot Int 2016;40(4):423–35.
[116] Jansen K, Steen Jensen J. Operative technique in knee disarticulation. Prosthet Orthot Int 1983;7:72–4.
[117] Theodorou DJ, Theodorou SJ, Kakitsubata Y. Skeletal muscle disease: patterns of MRI appearances. Br J Radiol 2012;85:e1298–308.
[118] Valero C, Javierre E, Garcia-Aznar JM, Menzel A, Gomez-Benito MJ. Challenges in the modeling of wound healing mechanisms in soft biological tissues. Ann Biomed Eng 2015;43(7):1654–65.
[119] Frossard L, Beck J, Dillon M, Evans J. Development and preliminary testing of a device for the direct measurement of forces and moments in the prosthetic limb of transfemoral amputees during activities of daily living. J Prosthet Orthot 2003;15:135–42.
[120] Koehler SR, Dhaher YY, Hansen AH. Cross-validation of a portable, six-degree-of-freedom load cell for use in lower-limb prosthetics research. J Biomech 2014;47(6):1542–7.
[121] Kobayashi T, Orendurff MS, Zhang M, Boone DA. Socket reaction moments in transtibial prostheses during walking at clinically perceived optimal alignment. Prosthet Orthot Int 2016;40(4):503–8.
[122] Highsmith MJ, Lura DJ, Carey SL, Mengelkoch LJ, Kim SH, Quillen WS, et al. Correlations between residual limb length and joint moments during sitting and standing movements in transfemoral amputees. Prosthet Orthot Int 2016;40(4):522–7.
[123] Sanders JE, Cagle JC, Harrison DS, Karchin A. Amputee socks: how does sock ply relate to sock thickness? Prosthet Orthot Int 2012;36(1):77–86.
[124] Cagle JC, D'Silva KJ, Hafner BJ, Harrison DS, Sanders JE. Amputee socks: sock thickness changes with normal use. Prosthet Orthot Int 2015;40(3):329–35.
[125] Schwarze M, Hurschler C, Seehaus F, Oehler S, Welke B. Loads on the prosthesis-socket interface of above-knee amputees during normal gait: validation of a multi-body simulation. J Biomech 2013;46:1201–6.

[126] Tang J, McGrath M, Laszczak P, Jiang L, Bader DL, Moser D, et al. Characterisation of dynamic couplings at lower limb residuum/socket interface using 3D motion capture. Med Eng & Physics 2015;37:1162–8.
[127] Rigney SM, Simmons A, Kark L. Concurrent multibody and finite element analysis of the lower-limb during amputee running. In: 37th annual international conference of the IEEE engineering in medicine and biology society (EMBC), Milan, Italy; 2015.
[128] Tuttle LJ, Sinacore DR, Mueller MJ. Intermuscular adipose tissue is muscle specific and associated with poor functional performance. J Aging Res 2012;2012:172957.
[129] Krouskop TA, Dougherty DR, Vinson FS. A pulsed Doppler ultrasonic system for making noninvasive measurements of the mechanical properties of soft tissue. J Rehab Res Dev 1987;24(2):1–8.
[130] Brown PG, Alsousou J, Cooper A, Thompson MS, Noble JA. The AutoQual ultrasound elastography method for quantitative assessment of lateral strain in post-rupture Achilles tendons. J Biomech 2013;46:2695–700.
[131] Park E, Maniatty AM. Shear modulus recontstruction in dynamic elastography: time harmonic case. Phys Med Biol 2006;51:3697–721.
[132] Dubuis L, Avril S, Debayle J, Badel P. Identification of the material parameters of soft tissues in the compressed leg. Comp Meth Biomech Biomed Eng 2012;15:3–11.
[133] Prompers JJ, Jeneson JAL, Drost MR, Oomens CCW, Strijkers GJ, Nicolay K. Dynamic MRS and MRI of skeletal muscle function and biomechanics. NMR Biomed 2006;19:927–53.
[134] Wheatley BB, Pietsch RB, Haut Donahue TL, Williams LN. Fully non-linear hyper-viscoelastic modeling of skeletal muscle in compression. Comp Meth Biomech Biomed Eng 2016;19(11):1181–9.
[135] Sanders J, Greve JM, Clinton C, Hafner BJ. Clinical study: changes in interface pressure and stump shape over time: preliminary results from a trans-tibial amputee subject. Prosthet Orthot Int 2000;24:163–8.
[136] Lilja M, Johansson S, Oberg T. Relaxed versus activated stump muscles during casting for trans-tibial prostheses. Prosthet Orthot Int 1999;23:13–20.
[137] Lee VSP, Gross P, Spence WD, Solomonidis SE, Paul JP. Two dimensional finite element model of a transverse section of the trans-femoral amputee's stump.. In: Computer methods in biomechanics & biomedical engineering -, 2; 1998.
[138] Rohan CP-Y, Badel P, Lun B, Rastel D, Avril S. Prediction of the biomechanical effects of compression therapy on deep veins using finite element modelling. Ann Biomed Eng 2014;43(2):314–24.
[139] Bolsterlee B, Veeger HEJ, van der Helm FCT, Gandevia SC, Herbert RD. Comparison of measurements of medial gastrocnemius architectural parameters from ultrasound and diffusion tensor images. J Biomech 2015;48:1133–40.
[140] Fernandez J, Alipour M, Shim V, Mithraratne K. A diffusion tensor imaging based model of muscle mechanics. In: XXIV congress of the international society of biomechanics, Brazil; 2013.
[141] Levya-Mendivil MF, Page A, Bressloff NW, Limbert G. A mechanistic insight into the mechanical role of the stratum corneum during stretching and compression of the skin. J Mech Behav Biomed Mater 2015;49:197–219.
[142] Loerakker S, Stekelenburg A, Strijkers GJ, Rijpkema JJM, Baaijens FPT, Bader DL, et al. Temporal effects of mechanical loading on deformation-induced damage in skeletal muscle tissue. Ann Biomed Eng 2010;38(8):2577–87.
[143] Loerakker S, Manders E, Strijkers GJ, Nicolay K, Baaijens FPT, Bader DL, et al. The effects of deformation, ischemia, and reperfusion on the development of muscle damage during prolonged loading. J Appl Phys 2011;111:1168–77.
[144] Loerakker S, Bader DL, Baaijens FPT, Oomens CWJ. Which factors influence the ability of a computational model to predict the in vivo deformation behaviour of skeletal muscle? Comput Methods Biol Med 2013;16(3):338–45.
[145] Linder-Ganz E, Shabshin N, Itzchak Y, Yizhar Z, Siev-Ner I, Gefen A. Strains and stresses in sub-dermal tissues of the buttocks are greater in paraplegics than in healthy during sitting. J Biomech 2008;41:567–80.
[146] de Wert LA, Bader DL, Oomens CWJ, Schoonhoven L, Poeze M, Bouvy ND. A new method to evaluate the effects of shear on the skin. Wound Repair Regen 2015;23:885–90.
[147] Worsley PR, Prudden G, Gower G, Bader DL. Investigating the effects of strap tension during non-invasive ventilation mask application: a combined biomechanical and biomarker approach. Med Dev: Evid Res 2016;9:409–17.
[148] Woodhouse M, Worsley PR, Voegeli D, Schoonhoven L, Bader DL. The physiological response of soft tissue to periodic repositioning as a strategy for pressure ulcer prevention. Clin Biomech 2015;30:166–74.
[149] Gray RJ, Worsley PR, Voegeli D, Bader DL. Monitoring contractile dermal lymphatic activity following uniaxial mechanical loading. Med Eng Phys 2016;38:895–903.
[150] Buis AWP, Convery P. Calibration problems encountered while monitoring stump/socket interface pressures with force sensing resistors: techniques adopted to minimise inaccuracies. Prosthet Orthot Int 1997;21:179–82.
[151] Convery P, Buis AWP. Conventional patellar-tendon-bearing (PTB) socket/stump interface dynamic pressure distributions recorded during the prosthetic stance phase of gait of a trans-tibial amputee. Prosthet Orthot Int 1998;22:193–8.
[152] Williams RB, Porter D, Roberts VC, Regan JF. Triaxial force transducer for investigating stresses at the stump/socket interface. Med Biol Eng Comput 1992;30:89–96.
[153] Jasni F, Hamzaid NA, Muthalif AGA, Zakaria Z, Shasmin HN, Ng S-C. In-socket sensory system for transfemoral amputees using piezoelectric sensors: an efficacy study. IEEE/ASME Trans Mechatron 2016;21(5):2466–76.
[154] Drewniak EI, Crisco JJ, Spenciner DB, Fleming BC. Accuracy of circular contact area measurements with thin-film pressure sensors. J Biomech 2007;40:2569–72.
[155] Laszczak P, Jiang L, Bader DL, Moser D, Zahedi S. Development and validation of a 3D-printed interfacial stress sensor for prosthetic applications. Med Eng Phys 2015;37:132–7.
[156] Sundara-Rajan K, Bestick A, Rowe GI, Klute GK, Ledoux WR, Wang HC, et al. An interfacial stress sensor for biomechanical applications. Meas Sci Technol 2012;23:085701.
[157] Laszczak P, McGrath M, Tang J, Gao J, Jiang L, Bader DL, et al. A pressure and shear sensor system for stress measurement at lower limb residuum/socket interface. Med Eng Phys 2016;38:695–700.
[158] Baldoli I, Mazzocchi T, Paoletti C, Ricotti L, Salvo P, Dini V, et al. Pressure mapping with textile sensors for compression therapy monitoring. Proc IMechE Part H: J Eng Med 2016;230(8):795–808.
[159] Al-Fakih EA, Abu Osman NA, Eshraghi A, Adikan FRM. The capability of Fiber Bragg Grating sensors to measure amputees' trans-tibial stump/socket interface pressures. Sensors 2013;13:10348–57.
[160] Tucker CJ, Wilken JM, Stinner DJ, Kirk KL. A comparison of limb-socket kinematics of bone-bridging and non-bone-bridging wartime transtibial amputations. J Bone Joint Surg [Am] 2012;94:924–30.
[161] Darter BJ, Sinitski K, Wilken JM. Axial bone-socket displacement for persons with a traumatic transtibial amputation: the effect of elevated vacuum suspension at progressive body-weight loads. Prosthet Orthot Int 2016;40(5):552–7.
[162] Breen A. A quantitative fluoroscopic study of the relationship between lumbar inter-vertebral and residual limb/socket kinematics in the coronal plane in adult male unilateral amputees. Institute of musculoskeletal research and clinical implementation. Anglo-European College of Chiropractic / Bournemouth University; 2015.
[163] Papaioannou G, Mitrogiannis C, Nianios G, Fiedler G. Assessment of amputee socket-stump-residual bone kinematics during strenuous activities using dynamic Roentgen stereogrammetric analysis. J Biomech 2010;43:871–8.
[164] Pare G, Elam JJ. Introducing information technology in the clinical setting. Int J Technol Assessm Health Care 1998;14(2):331–43.
[165] Mytton OT, Velazquez A, Banken R, Matthew JL, Ikonen TS, Taylor K, et al. Introducing new technology safely. Qual Saf Health Care 2010;19(S2):i9–i14.
[166] Rivlin RS. Large elastic deformations of isotropic materials. IV. Further developments of the general theory. Phil Trans R Soc A 1948;241(835):379–97.
[167] Treloar LRG. The elasticity of a network of long-chain molecules - II. Trans Faraday Soc 1943;39:241–6.
[168] Treloar LRG. Stress-strain data for vulcanised rubber under various types of deformation. Trans Faraday Soc 1944;40:59–70.
[169] Mooney MA. A theory of large elastic deformation. J Appl Phys 1940;11:582–92.
[170] Ogden RW. Large deformation isotropic elasticity - on the correlation of theory and experiment for incompressible rubberlike solids. Proc R Soc Lond A 1972;326:565–84.
[171] Yeoh OH. Some forms of the strain energy function for rubber. Rubber Chem Technol 1993;66(5):754–71.
[172] Pickard-Gabriel CJ, Ledford CL, Gajewski DA, Granville RR, Andersen RC. Traumatic Transfemoral Amputation with Concomitant Ipsilateral Proximal Femoral Fracture. J Bone Joint Surg Am 2007;89(12):2764–8. doi:10.2106/JBJS.G.00229.
[173] Overman A, Potter BK. Alternative bone graft sources and techniques for tibiofibular synostosis creation following transtibial amputation. JBJS Case Connect 2015;5(1):e18.
[174] Khemka A, Frossard L, Lord S, Bosley B, Al Muderis M. Osseointegrated total knee replacement connected to a lower limb prosthesis: 4 cases. Acta Othopaedica 2013;86(6):740–4.
[175] Dunn MG, Silver FH, Swann DA. Mechanical analysis of hypertrophic scar tissue: structural basis for apparent increased rigidity. J Invest Dermatol 1985;84(1):9–13.
[176] Gefen A, Haberman E. Viscoelastic properties of ovine adipose tissue covering the gluteus muscles. J Biomech Eng 2007;129(6):924–30.
[177] Gefen A, Dilmoney B. Mechanics of the normal woman's breast. Technol Health Care 2007;15(4):259–71.
[178] Hoyt K, Kneezel T, Castaneda B, Parker KJ. Quantitative sonoelastography for the in vivo assessment of skeletal muscle viscoelasticity. Phys Med Biol 2008;53(15):4063–80.
[179] Lemmon D, Shiang TY, Hashmi A, Ulbrecht JS, Cavanagh PR. The effect of insoles in therapeutic footwear - a finite element approach. J Biomech 1997;30(6):615–20.